Journal of the Mechanics and Physics of Solids 109 (2017) 264–287

Contents lists available at ScienceDirect

Journal of the Mechanics and Physics of Solids

journal homepage: www.elsevier.com/locate/jmps

Fishnet statistics for probabilistic strength and scaling of nacreous imbricated lamellar materials

Wen Luo[a], Zdeněk P. Bažant[b,*]

[a] Northwestern University, USA
[b] Department of Civil and Environmental Engineering, Northwestern University, 2145 Sheridan Road, CEE/A135, Evanston, IL 60208, USA

ARTICLE INFO

Article history:
Received 2 July 2017
Accepted 29 July 2017
Available online 1 September 2017

Keywords:
Structural safety
Probabilistic mechanics
Nacre
Biomimetic materials
Random strength
Probability distribution tail
Imbricated lamellar structures
Staggered platelet structures
Monte Carlo simulations
Failure risk
Fracture
Brick and mortar structures

ABSTRACT

Similar to nacre (or brick masonry), imbricated (or staggered) lamellar structures are widely found in nature and man-made materials, and are of interest for biomimetics. They can achieve high defect insensitivity and fracture toughness, as demonstrated in previous studies. But the probability distribution with a realistic far-left tail is apparently unknown. Here, strictly for statistical purposes, the microstructure of nacre is approximated by a diagonally pulled fishnet with quasibrittle links representing the shear bonds between parallel lamellae (or platelets). The probability distribution of fishnet strength is calculated as a sum of a rapidly convergent series of the failure probabilities after the rupture of one, two, three, etc., links. Each of them represents a combination of joint probabilities and of additive probabilities of disjoint events, modified near the zone of failed links by the stress redistributions caused by previously failed links. Based on previous nano- and multi-scale studies at Northwestern, the strength distribution of each link, characterizing the interlamellar shear bond, is assumed to be a Gauss-Weibull graft, but with a deeper Weibull tail than in Type 1 failure of non-imbricated quasibrittle materials. The autocorrelation length is considered equal to the link length. The size of the zone of failed links at maximum load increases with the coefficient of variation (CoV) of link strength, and also with fishnet size. With an increasing width-to-length aspect ratio, a rectangular fishnet gradually transits from the weakest-link chain to the fiber bundle, as the limit cases. The fishnet strength at failure probability 10^{-6} grows with the width-to-length ratio. For a square fishnet boundary, the strength at 10^{-6} failure probability is about 11% higher, while at fixed load the failure probability is about 25-times higher than it is for the non-imbricated case. This is a major safety advantage of the fishnet architecture over particulate or fiber reinforced materials. There is also a strong size effect, partly similar to that of Type 1 while the curves of log-strength versus log-size for different sizes could cross each other. The predicted behavior is verified by about a million Monte Carlo simulations for each of many fishnet geometries, sizes and CoVs of link strength. In addition to the weakest-link or fiber bundle, the fishnet becomes the third analytically tractable statistical model of structural strength, and has the former two as limit cases.

* Corresponding author.
E-mail address: z-bazant@northwestern.edu (Z.P. Bažant).

http://dx.doi.org/10.1016/j.jmps.2017.07.023
0022-5096/

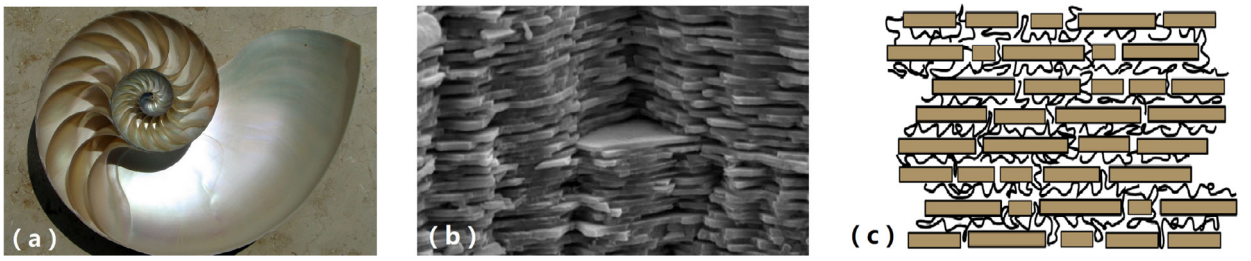

Fig. 1. a) Picture of nacre inside a nautilus shell; b) Electron microscopy image of a fractured surface of nacre; c) Microstructure of nacre (schematic, not to scale). The typical length of lamellae is 600 nm, thickness about 10 nm, and the thickness of polymer bonding layers about 0.5 nm) (all three images are from Wikipedia; https://en.wikipedia.org/wiki/Nacre).

1. Introduction

In spite of their weak brittle constituents, nacre-like imbricated (staggered) lamellar structures can attain very high strength and fracture energy. The reasons have been clarified in a host of studies of the mechanics of failure (e.g. Gao et al., 2003; Wang et al., 2001; Wei et al., 2015; Shao et al., 2012; Bertalan et al., 2014; Askarinejad and Rahbar, 2015).

These studies, however, were mostly deterministic and provided only the mean behavior. For nacreous structures, no realistic probability distribution of the strength with the far left fail seems to exist at present, yet this is where the 'devil' resides. To capture the tail is the goal of this study (whose main ideas were presented in a preliminary posting on ArXiv (Luo and Bažant, 2017)).

To design safe structures with nacre-mimetic materials typically requires knowing their strength distribution up to the tail with failure probability of about $P_f = 10^{-6}$ (per lifetime). This is generally the level of safety required for engineering structures such as bridges, aircraft, MEMS, etc. It ensures the risks of engineering structures to be three orders magnitude lower than other risks that people willingly or inevitably take (e.g., car driving), and to be of about the same level as the risk of being killed, e.g., by a lightning of falling tree. Such low tail probabilities can hardly be determined by histogram testing of strength of many identical specimens of structures.

The stochastic finite element method, as it exists, cannot furnish the far-out probability tail. It can hardly provide more than the mean and coefficient of variation of structure strength. How to extrapolate it to the far our tail is a crucial question. Its importance becomes clear by noting that the ratio of the failure loads of probability 10^{-6} extrapolated by means of Weibull or Gaussian (i.e., normal) distributions is about 2:1, and this translates into the same ratio of the required safety factors.

Consequently, one needs a realistic mathematical model for the strength distribution, to be verified only indirectly, by predictions depending on the tail. Here a diagonally pulled fishnet is proposed as the basis of such a model, providing a sufficiently realistic simplification of nacre's microstructure for which the probability distribution is analytically tractable.

The new idea of this article is to model the tail probability of strength of nacre-like structures by a square fishnet pulled along one of the diagonals. Same as the weakest-link model, the failure probability of fishnet, P_f, is obtained by calculating its counterpart—the survival probability, $1 - P_f$. The key point of analytical solution is to decompose the total survival probability into a sum of survival probabilities corresponding to the failures of one link, two links, three links, etc., restricted by joint probability of survival of all the other links. As will be shown, these added survival probabilities greatly enhance the strength for $P_f < 10^{-6}$, compared to the weakest-link model.

The analytical predictions of failure probability are here verified by millions of Monte-Carlo simulations. Monte Carlo simulations of nacreous structures have previously been conducted with the random fuse model (RFM) (Alava et al., 2006; Bertalan et al., 2014), in which the brittle bonds in the structure are simplified as a lattice of resisters with random burnout thresholds. The RFM simulates the gradual failure of resister network under increasing voltage. This is similar to the failure process of quasibrittle elastic material under controlled uniaxial load.

To calculate the maximum loads of the system of fishnet links, a simple finite element (FE) program for a pin-jointed truss is developed (in MatLab). For each of many shapes and sizes of the fishnet, the maximum loads are calculated for about 1 million input samples of randomly generated strengths of the links. Running each set of about 1 million FE solutions takes a few days. With such a large number of random samples, the resulting strength histograms become visually indistinguishable from the theoretical cumulative probability density function (cdf) of failure probability P_f.

2. Previous studies

The high strength and fracture toughness of nacre-like materials with "brick-and-mortar" structures (Fig. 1) has already been explained and demonstrated by a number of researchers. E.g., Wang et al. (2001) showed that the nano-asperities on the platelets (or lamellae) of hydrated nacre are the main cause of high resistance during the sliding of platelets and the robust mechanical behavior on the macro-scale. Gao et al. (2003) found that the stress concentrations at flaws and the damage in nacre are significantly mitigated on the nano-scale. Shao et al. (2012) demonstrated that the fracture toughness

of nacre is greatly enhanced by the crack bridging effects in the staggered microstructure. Dutta et al. (2013, 2014) clarified the role of overlap of adjacent lamellae in impact dynamics of nacreous layers.

On the other hand, studies of the statistical aspects of the nacreous (or 'brick-and-mortar') structures have been rare, especially in regard to the type and tail of the probability distribution of strength. No undisputed theoretical formulation has been established so far. General quasi-brittle structures have usually been considered to follow the weakest-link model, and its limiting distribution for an infinite number of links ($N \to \infty$), which is the Weibull distribution, has commonly been assumed. However, when the representative volume elements (RVE) of material are not negligible compared to the structure size, the finite weakest-link model (Bažant and Le, 2017; Bažant and Pang, 2006; 2007; Le and Bažant, 2009; 2011) (with finite N) has been shown to apply instead.

Meanwhile, limitations of the classical Weibull-type statistics have long been realized. A theory of the finite weakest-link model has been developed beginning 2006 (Bažant, 2005; Bažant and Le, 2009; 2017; Bažant and Pang, 2006; 2007; Bažant and Planas, 1998; Bažant and Xi, 1991; Le and Bažant, 2011; Le and Bažant, 2012; Le et al., 2009; 2011; Pang et al., 2008; Salviato and Bažant, 2014; Salviato et al., 2014). Applicability of the infinite weakest-link chain model has later also been questioned by Bertalan et al. (2014). As revealed by Monte Carlo simulations in Bažant and Pang (2006); 2007), Le et al. (2011) and Bertalan et al. (2014), the failure probability, P_f, deviates significantly from the mean fit by Weibull distribution for small nominal stresses, and thus for low P_f. Yet, in structural design, the lower tail of P_f is what is most important.

According to the weakest-link model, the failure load occurs immediately after one representative volume of material (RVE) fails (in this study, we consider the load to be controlled, in which case the maximum load, or load capacity, is the failure load). Such immediate failure neglects the parallel couplings due to lateral strain compatibility between parallel material elements and the associated stress redistributions causing a release of stored energy due to crack growth. On the RVE level, such interactions have been taken into account in the hierarchical model of series and parallel couplings within the RVE of a quasibrittle particulate material (Bažant, 2005; Bažant and Pang, 2006; 2007; Le and Bažant, 2011; Le et al., 2011). However, as will be seen, such a hierarchical model is not the best approximation for nacre.

Unlike the weakest-link model, the fiber bundle model takes into account the effect of stress redistribution. It was studied rigorously by Daniels (1945), who assumed the rule of equal load sharing and showed the maximum load (or failure probability in case of load control) to converge to the normal (or Gaussian) distribution as the number of fibers tends to infinity (a proof for arbitrary postpeak softening of fibers is given below Eq. (5.5.3) in Bažant and Le (2017)).

Later, a chain-of-bundles model was conceived by Harlow and Phoenix (1978a); 1978b), to estimate the failure probability distribution of fibrous composites under uniaxial tension. They assumed the cross sections of the composite with certain finite spacing along the loading direction to be statistically independent. Further they assumed these cross sections to be related to each other through a series coupling in a chain and the individual cross sections to be treated as bundles. However, unlike the present study, the local load-sharing rule for their bundles was intuitive, hypothetical, rather than based on mechanics. A significant deviation of P_f from the Weibull distribution was predicted. Due to overwhelming obstacles for large scale numerical simulations at that time (1978), only bundles with less than 10 fibers were analyzed, and no verification through Monte Carlo simulations could be given.

It should be mentioned that, for the sake of simplifying the deterministic analysis of fracture toughening of nacre, a fishnet truss was already introduced in Askarinejad and Rahbar (2015), as a simple replacement of the interlaminar shear bonding. This truss was combined with the imbricated system of stiff lamellae, which had tensile connections between the ends of lamellae in the same row.

3. Statistical modeling of fishnet structure

In nature, the mechanical responses of hydrated and dry nacres are quite different: A hydrated nacre like that in the shell of pearl oysters and abalones exhibits strong nonlinearity and a yielding plateau under tension, compression and shear (Wang et al., 2001). However, dry nacre is mostly brittle and its ductility under uniaxial tension as well as compression is vanishingly small. In this paper, only a dry (and brittle) nacre is considered. Its behavior up to brittle failure at maximum load may be treated as linearly elastic.

3.1. Fishnet—proposed probabilistic approximation of nacre failure

To simplify the essence of load transmission in the staggered imbricated structure of nacreous materials, we ignore the relatively weak longitudinal connections of adjacent lamellae (or platelets) in the same row, and assume that most of the strength and stiffness is provided by the shear bonds between parallel lamellae (Fig. 2a). If we are interested in the longitudinal strength of nacre under tensile load parallel to the lamellae, the transverse normal stiffness of the thin polymer layers, providing transverse connections of the lamellae, does not play a significant role. So, to model the probability of failure under longitudinal tension, we may imagine that the lamellae are replaced by nodes at their centroids, shown as the dark dots in Fig. 2a, and that the nodes are connected by bars, or links (dashed lines in Fig. 2a) transmitting only axial forces.

Thus, to represent the connectivity in an idealized regular array of identical lamellae, we have a system of nodes and links shown in Fig. 2b, which is equivalent to a truss. This truss looks like a fishnet. For example, in Fig. 2(a), the lamellae

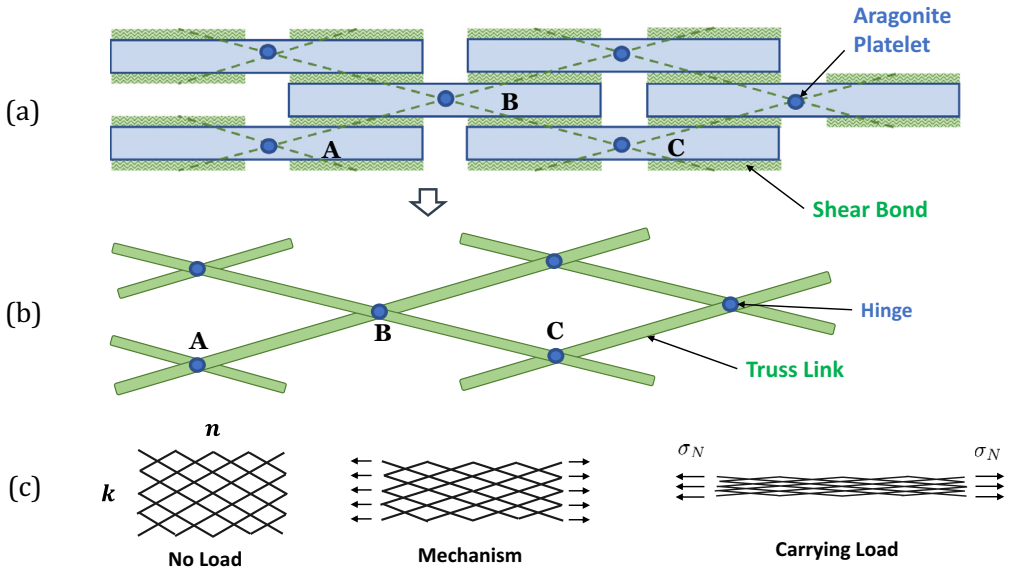

Fig. 2. a) Schematic illustration of microstructure of nacre; b) Equivalent fishnet structure; c) Deformation mechanism and lateral contraction of fishnet (transversely unpropped).

(or platelets) A, B and C are mapped to nodes A, B and C in Fig. 2b and the shear bonds AB and AC in Fig. 2a are replaced by quasibrittle truss elements, or links, AB and AC in Fig. 2b, respectively. This is equivalent to pulling an elastic fishnet along the longitudinal diagonals of the parallelogram cells.

In real nacre, of course, the array of lamellae is not regular since the overlaps of lamellae are random and nonsymmetric. This irregularity introduces high scatter of nacre strength. As we will see, the scatter is rather helpful for safety. Since a regular fishnet is simpler to analyze, we will replace the scatter due geometrical irregularity of nacre with a scatter of the link strength. Thus the random scatter of strength will be assumed to be much higher than in pure aragonite (a form of $CaCO_3$) or the biopolymeric binder, the main constituents of nacre. The most important feature for statistical behavior is that, regardless of fishnet regularity or irregularity, the link connectivity in the diagonally pulled fishnet appears to capture the mixture of longitudinal (or series) and transverse (or parallel) connections.

The fishnet truss is not statically determinate. The parallelograms in the fishnet form a mechanism which will, under longitudinal tension, shrink immediately at the start of loading into a set of coinciding lines (or fibers) with staggered (or imbricated) connections among them (Fig. 2c). Evidently, this is a simplification. Nevertheless, it retains the essence of transverse interactions between the adjacent rows of lamellae. This simplification could be avoided by propping each fishnet square with transverse diagonal compression struts. This complication, however, would not change the statistics appreciably. For the purpose of illustration, the stress field in the fishnet will here be always displayed in the original (Lagragian) coordinates, i.e., in the initial state before the fishnet collapse into coinciding lines.

The topological connectivity of fishnet and its stress redistribution plays a key role in the failure probability. This is what makes the statistical model fundamentally different from each of the other two basic models for failure statistics, namely the weakest-link chain and the fiber bundle.

3.2. Stress redistribution near the link failure zone

The failure probability of a fishnet obviously depends on the stress redistributions after successive link failures. First we consider the maximum load (or failure under load control) to be reached after the failure of one link only. We assume the strength of all links to be independent and identically distributed (i.i.d.) random variables (this implies that the autocorrelation length of the random strength field is assumed to be equal to the length of the link, which is, of course, a simplifying assumption, but probably a good one). The perimeter length of a set of geometrically similar fishnet structures is proportional to the structure size, D, while the area of the fishnet structure is proportional to D^2. Thus the probability of the failed link to be located exactly on the boundary tends to zero as $D \to \infty$. Therefore, for large enough fishnets, the first link to fail must lie, with probability almost 1, in the fishnet interior. So we consider here only the case of link failures in the fishnet interior.

3.2.1. Stress redistribution in equivalent fishnet continuum

To simplify the stress redistribution analysis, fishnets consisting of many links may be treated as a continuum. To formulate the governing differential equation, we consider a fishnet whose initial configuration consists of orthogonal lines of links (Fig. 3a), and introduce Lagrangian coordinates (ξ, η) parallel to link lines. After the collapse of the fishnet into one

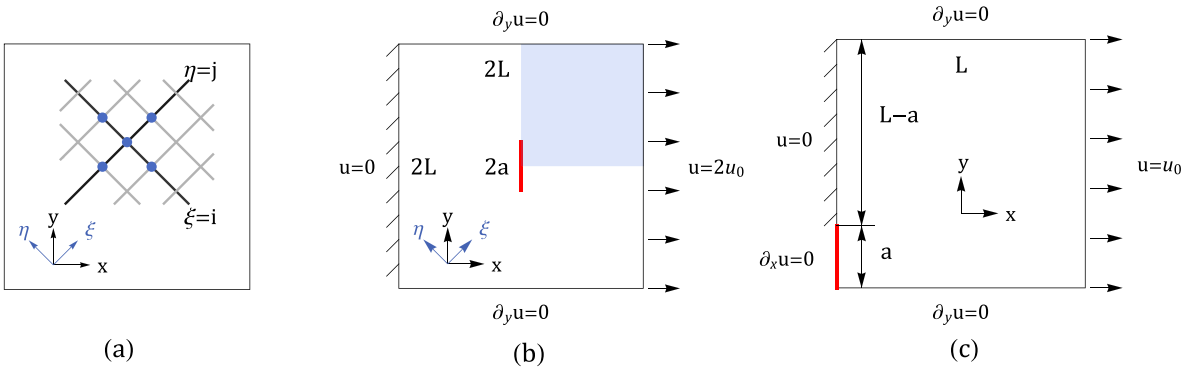

Fig. 3. a) Two orthogonal coordinate systems, (x, y) and (ξ, η); b) Configuration of fishnet continuum with a pre-existing crack ; c) one quarter (shadowed region) of the fishnet continuum shown in (b).

line, all the four links connected to one node (i, j) become coincident and parallel, aligned in the x-direction. Since the initial fishnet state is kinematically indeterminate and represents a mechanism, the equilibrium condition of a node must be written for the collapsed state of fishnet. Equilibrium requires that the sum of the forces in the x direction, applied from the four links acting on node i, j, would vanish. This leads to the difference equation:

$$\frac{EA}{a}\left(\frac{u_{i,j+1}-u_{i,j}}{a}+\frac{u_{i,j-1}-u_{i,j}}{a}+\frac{u_{i+1,j}-u_{i,j}}{a}+\frac{u_{i-1,j}-u_{i,j}}{a}\right)=0 \tag{1}$$

where $u_{i,j}$ = displacement in the x direction of any joint (i, j), a = length of each link, E = Young's modulus and A = cross section area of the link.

To obtain the continuum limit of $a \to 0$, consider now the Lagrangian coordinates (ξ, η) in the initial directions of the links, i.e., before fishnet collapse (Fig. 3a). Obviously, the continuum limit is the partial differential equation:

$$\frac{\partial^2 u}{\partial \xi^2}+\frac{\partial^2 u}{\partial \eta^2}=0 \quad \text{or} \quad \nabla^2_{(\xi,\eta)}u=0 \tag{2}$$

which is the Laplace equation. Since the Laplacian ∇^2 is invariant at coordinate rotations, the differential equation of equilibrium in the x direction in the initial (x, y) coordinates before fishnet collapse reads:

$$\frac{\partial^2 u}{\partial x^2}+\frac{\partial^2 u}{\partial y^2}=0 \quad \text{or} \quad \nabla^2_{(x,y)}u=0 \tag{3}$$

where x is the direction of loading of the fishnet and y is the transverse direction with no load.

Note that if we defined the (ξ, η) coordinate system in the deformed configuration (in which all the links become parallel and coincident with one line), the governing equation would become $d^2u/dx^2 = 0$, which is independent of transverse direction y. Then, in the collapsed configuration, we would have to distinguish the coincident link lines by numbers rather than by y and deal with a system of ordinary differential equations instead of one partial differential equation. Although this description would be equivalent, it would be inconvenient.

There are many possibilities of failure of one link or one group of links. Considering them in the discrete form would excessively complicate the calculation of failure probabilities. Therefore we analyze the stress redistributions in the approximate overall sense by the continuum defined by Eq. (3).

The simplest case is a failure of a group of links approximated as a circular hole of radius R_0. Converting the partially differential equation to polar coordinates (R, θ), we have $(\partial^2 u/\partial R^2) + (1/R)(\partial u/\partial R) = 0$, and seeking an axisymmetric solution (for the obvious boundary conditions), we readily find that, according to the continuum approximation, the smeared continuum link strains $\partial u/\partial R$, as well as the stresses, decay from the hole as R_0/R where R_0 is the characteristic length of decay, proportional to the hole size.

The case of a sharp crack of length $2a$ in the continuum is slightly different. The displacement near the crack tip may be sought in the separated form $u = f(\theta)R^{\lambda}$ in which (R, ϕ) are the polar coordinates centered at the crack tip. Upon substitution into Eq. (3), it is concluded that, like in linear elastic fracture mechanics (LEFM), the strains and stresses near the crack tip (i.e., for $R \to 0$) decay as $(R/R_0)^{-1/2}$ where the characteristic length R_0 is proportional to the crack length $2a$. But far away from the crack (i.e., for $R \to \infty$), the stresses decay as $(R/R_1)^{-2}$ where R_1 is again a characteristic length proportional to $2a$. What is important is that the disturbance caused by the failed links is localized and decays to a negligible value within a certain finite distance.

Fig. 4 shows the finite element results for constant stress contours of a fishnet continuum with a sharp crack of different lengths (a = 1,2,3,4). One can see that the stresses fluctuate rapidly only near the crack tip and are much more uniform farther away from the crack. This verifies the rapid decay assumption.

In the continuum approximation, the regions near the faces of the crack are shielded from the load and get unloaded to near-zero. Later they will be seen to complicate the probabilistic analysis, compared to the classical weakest-link and fiber-

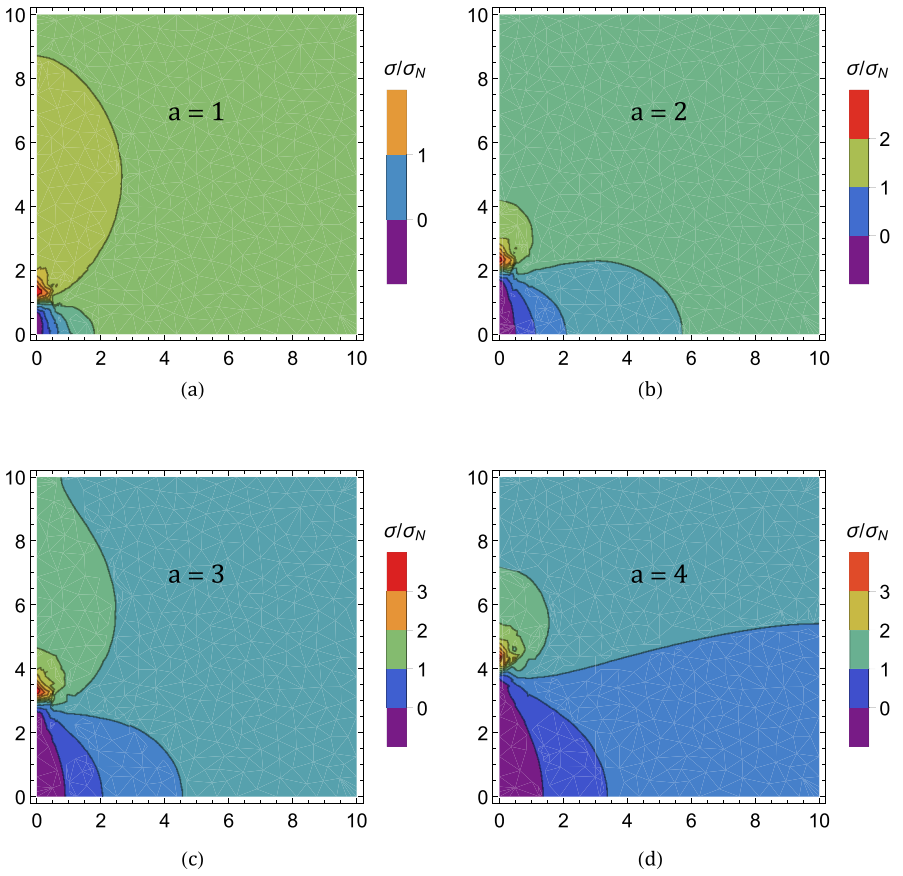

Fig. 4. Profiles of relative stress $\eta = \sigma/\sigma_N$ of fishnet continuum for different crack lengths: $a = 1$, 2, 3 and 4, calculated for $L = 10$.

bundle models. This is the trade-off that must be accepted to make it possible to calculate the tail of failure probability distribution of nacreous materials analytically.

3.2.2. Stress redistribution within the discrete fishnet

Knowing the asymptotic stress distribution near a crack (i.e., near one or more failed links) helps to estimate the failure probability more accurately, but the exact discrete redistributed stress field must be calculated numerically. This is easily done by the finite element method; see the results in Fig. 5. Fig. 5a shows the stress field in a square fishnet with 64×64 links under uniform horizontal tension. The properties of all links are considered to be uniform. One of the links is assumed to be already failed before the maximum load, prior to any loading. Except close to this link, the stresses are almost uniform.

To render the detail near the damage zone (specifically, inside the marked square), Fig. 5b presents a schematic showing the stresses in that zone only. We see that 10 close neighbors of the failed link endure stress redistributions with stresses magnified by more than 10%; $\eta_{max} = \sigma_{max}/\sigma = 1.6$ and $\eta_{min} = \sigma_{min}/\sigma = 0.64$. Numbers next to the highlighted links are their normalized stresses σ/σ_{max}. Apart from these 10 marked links around the failed one, all the other links undergo stress redistributions smaller than 10%. The stress amplification zone is shaded lightly, and the stress shielding (or unloading) zone is unshaded.

As an example of how the stress ratio η tends to 1 while moving from the boundary toward the failed link, $\eta = \sigma/\sigma_N$ is plotted versus the link number along the typical cross-section through the failed link in Fig. 5c. Here the thresholds $|\eta - 1| = 5\%$ and $|\eta - 1| = 10\%$ are indicated by horizontal solid and dashed lines, respectively. Among 64 links along the cross-section, the case $|\eta - 1| > 5\%$ occurs in less than 5 links. The stress disturbance due to a failed link decays to a negligible value (less than 5%) within the distance of 4 links. Later the values of η near the crack tip are needed to calculate the failure probability of the fishnet.

3.3. Two basic models of strength statistics: weakest-link chain and fiber-bundle

Before embarking on fishnet statistics, we need to review the basics of these two classical models for strength probability. First consider a chain of n identical links under tensile stress σ whose strengths represent i.i.d. random variables. The idea is to focus on survival instead of failure. For the whole chain to survive, every single link must survive. According to the

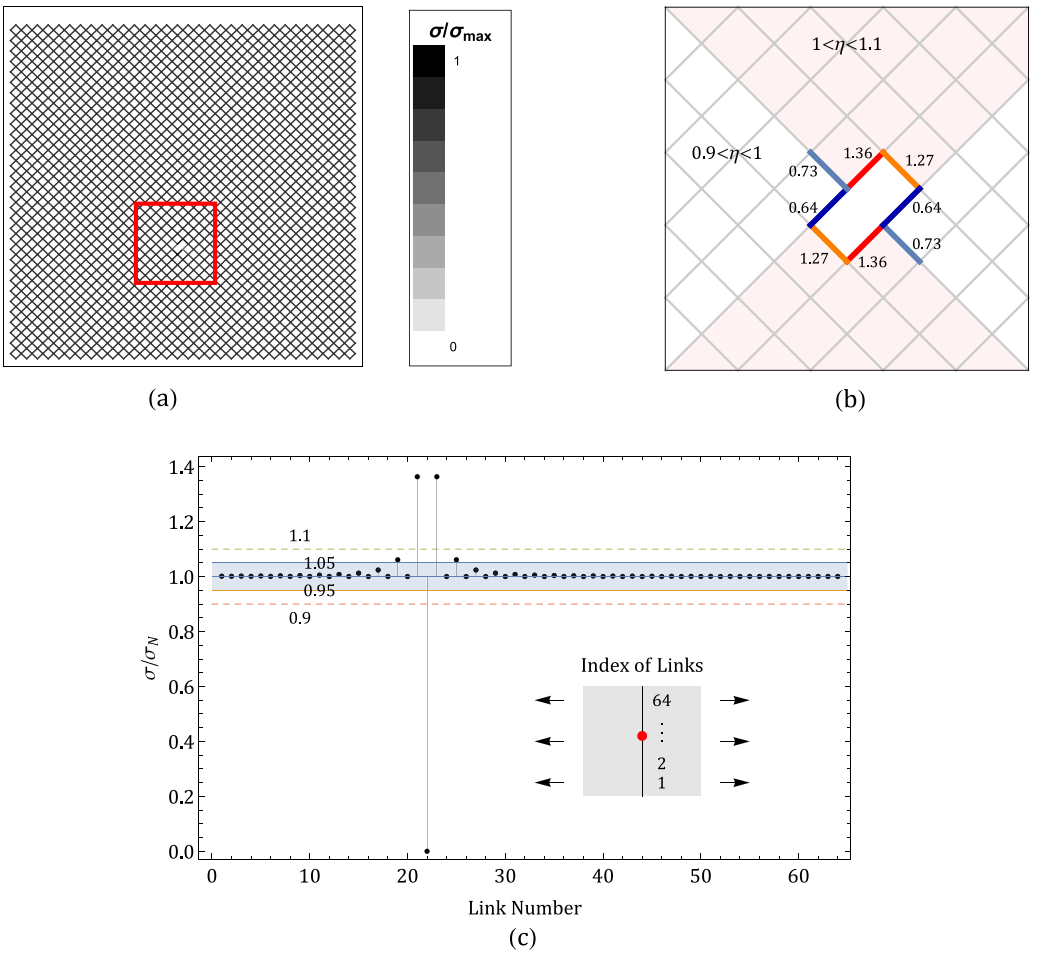

Fig. 5. a) Normalized stress profile of fishnet with one failed link on the inside; b) Schematic showing the stress ratios ($\eta = \sigma/\sigma_N$) in the highlighted region of (a); c) Stress ratios of each link along the vertical cross-section through the failed link in (a) indexed by the link number in FE simulation.

joint probability theorem, this condition yields:

$$1 - P_f(\sigma) = [1 - P_1(\sigma)]^n \tag{4}$$

where P_1 and P_f are the failure probabilities of a single link and of the whole chain, respectively. The limit of this equation for $n \to \infty$ may be written as

$$1 - P_f(\sigma) = \lim_{n\to\infty} (1 - x/n)^n = e^{-x}, \quad x = nP_1(\sigma)$$

What is the $P_1(\sigma)$ distribution for an RVE of the material? There are two different arguments showing that the distribution tail must be a power law:

1. Physically, analysis of nanoscale fracture on the basis of Kramer's transition rate theory showed that the tail must be a power law, and analysis of the scale transitions up to the macro-scale of the RVE of material showed that the power law tail is preserved across the scales while its exponent is greatly increased (Bažant and Le, 2009; 2017; Bažant et al., 2009; Bažant and Pang, 2006; 2007).
2. According to the stability postulate of extreme value statistics (Fisher and Tippett, 1928), the type of the distribution for $\sigma \to \infty$ must be invariant upon linear transformation of the independent variable σ. One may check that this condition is verified if the left tail of P_1 is a power law, $P_1(\sigma) = \alpha\sigma^m$, where m and α are constants. But is that the only possibility? It is, according to the stability postulate (Fisher and Tippett, 1928). Without considering the sign of σ, there would be three and only three possibilities, but the condition that the tensile strength σ cannot be negative leaves only one possibility, the power-law tail (which has also been extensively verified experimentally). This leads, for a structure with an infinite number of RVE's, to the Weibull distribution

$$P_f(\sigma) = 1 - e^{-\alpha\sigma^m} \tag{5}$$

where m is called the Weibull modulus (or shape parameter) and α is the scale parameter.

For a chain with finite number of links, only the left portion of the distribution of $P_f(\sigma)$ is Weibullian. The rest is approximately Gaussian and gradually shrinks as the Weibullian portion grows at increasing N (Bažant and Pang, 2006; Le et al., 2011).

The fiber bundle model is a reasonable approximation for cables but has sometimes also been applied to fiber composites and other materials, even though it does not represent their failure statistics realistically. In contrast to a chain, the fiber bundle reaches the maximum load (or failure under load control) only after the breakage of many fibers. After each fiber break, the load redistributes among the surviving fibers according to the stiffness of the fiber and of the support by the surrounding structure. The redistribution rules have often been purely intuitive, but here we insist on defining the redistribution by mechanics, considering perfectly rigid and non-rotating loading platens, which gives what is called equal load sharing. As proven by Daniels (1945), the distribution of the total load carried by such a bundle converges to the Gaussian (or normal) distribution.

3.4. Fishnet statistics

3.4.1. Extension of weakest link model

We will study a general (two-dimensional) fishnet consisting of many links whose failure probabilities s_i are i.i.d. random variables. In contrast to a chain, more than one link may fail before the fishnet reaches the maximum load. Therefore, we define the random variable $X(\sigma)$ = number of links that have failed after uniform stress σ is imposed at the fishnet boundary. $X(\sigma)$ is measured up to the end of loading at which no more damages occur.

Now consider a fishnet with $N = k \times n$ links (Fig. 2c), i.e., with k rows and n columns, pulled in the direction of rows. Since events $\{X(\sigma) = r\},\ r = 0, 1, \ldots,$ are mutually exclusive, the whole sample space can be partitioned by these mutually exclusive (or disjoint) events into $N+1$ subsets: $\{X(\sigma) = r\}, r = 0, 1, \cdots, N$. In contrast to a chain or a fiber bundle, the failure of a fishnet, however, cannot be characterized as either $\{X(\sigma) = 1\}$, $\{X(\sigma) = k\}$ or $\{X(\sigma) = N\}$ because the failure also depends on the position of the failed links.

The whole fishnet reaches the maximum load (and thus would fail if the load were controlled) when sufficiently many links fail. As more links fail in the post-peak range, the load finally drops to 0. At that moment, a part of the failed links must form a contiguous crack cutting through all the k rows. Thus the condition $X(\sigma) \geq k$ is necessary for total failure (load drop to zero). But it is not sufficient. If all the damages (greater then k) are scattered without forming a full crack, the structure has not failed completely and has a higher strength than the load applied. Based on these considerations, the probability of fishnet survival may be expressed as:

$$\begin{aligned} 1 - P_f(\sigma) =& P_{S_0}(\sigma) + P_{S_1}(\sigma) + P_{S_2}(\sigma) + \cdots + P_{S_{k-1}}(\sigma) \\ &+ \mathbb{P}(X(\sigma) \geq k \ \text{ while the whole structure has not yet failed}) \end{aligned} \tag{6}$$

where $P_f(\sigma) = \mathbb{P}(\sigma_{max} \leq \sigma)$, σ_{max} = nominal strength of structure; and $P_{S_r}(\sigma) = \mathbb{P}(X(\sigma) = r),\ r = 0, 1, 2, \ldots, N$. Since the event $\{X(\sigma) = 0\}$ means that no link can fail under the load σ, we have

$$P_{S_0}(\sigma) = [1 - P_1(\sigma)]^N \quad \text{where} \quad P_1(\sigma) = \mathbb{P}(s_i \leq \sigma). \tag{7}$$

If we consider only the first term P_{S_0} on the right-hand side of Eq. (6), the model is equivalent to the classical weakest-link model, i.e.,

$$1 - P_f(\sigma) = P_{S_0}(\sigma) = [1 - P_1(\sigma)]^N \tag{8}$$

This may be imagined as rearranging all the links into a chain with only 1 row and N columns.

Because the other terms in the sum of Eq. (6) are excluded, the weakest-link model gives a strict upper bound on the failure probability of the fishnet.

3.4.2. Two-term fishnet statistics

To get a better approximation, let us now truncate the sum in Eq. (6) after the second term P_{S_1}. Let σ_N be the nominal stress representing the average stress in the cross section of the fishnet, and σ_i be the stress in the ith link when the nominal stress is $\sigma_N = \sigma$. Also denote $\eta_i = \sigma_i/\sigma_N$, which is the relative stress (or stress ratio) in link i after some links have failed. Based on the previous analysis of stress redistribution, we assume η_i not to depend on the position of the failed link. For the two-term model, the survival probability is

$$1 - P_f(\sigma) = P_{S_0}(\sigma) + P_{S_1}(\sigma), \tag{9}$$

where P_{S_0} is given by Eq. (7), and $P_{S_1}(\sigma)$ is the probability that, under load $\sigma_N = \sigma$, only one link has failed (i.e., all the others have survived). This event can be further decomposed as the union of N mutually exclusive events:

$$\{X(\sigma) = 1\} = \bigcup_{i=1}^{N} \Omega_i, \tag{10}$$

where Ω_i is the event that the ith link is the one and only one that has failed under the loading $\sigma_N = \sigma$. Next, we define a family of events for every single link:

$$\omega_i(\sigma) = \text{the } i\text{th link survives under stress } \sigma_i \text{ equal to } \sigma \tag{11}$$

Then the event Ω_i that the ith link fails while all the others survive is equivalent to

$$\Omega_i = \omega_i^c(\sigma) \cap \left\{ \bigcap_{j\neq i} \left[\omega_j(\sigma) \cap \omega_j(\eta_j^{(1)}\sigma) \right] \right\} \tag{12}$$

where $\omega_i^c(\sigma)$ is the event that the ith link fails under the initial stress field $\sigma_i = \sigma$. The expression $\bigcap_{j\neq i}\left[\omega_j(\sigma)\cap\omega_j(\eta_j^{(1)}\sigma)\right]$ represents the event that the remaining links survive under both the initial and redistributed stresses. Hence the expression for P_{S_k} is:

$$P_{S_1}(\sigma) = \mathbb{P}\{X(\sigma)=1\} = \mathbb{P}\{\cup_{i=1}^N \Omega_i\} = \sum_{i=1}^N \mathbb{P}\{\Omega_i\} \tag{13}$$

$$= N\cdot\mathbb{P}\left\{ \omega_i^c(\sigma) \cap \left[\bigcap_{j\neq i} \left(\omega_j(\sigma)\cap\omega_j(\eta_j^{(1)}\sigma) \right) \right] \right\} \tag{14}$$

Consider now that the strengths of links $P_1(\sigma) = \mathbb{P}\{\omega_i(\sigma)\}$ are i.i.d. random variables. Then Eq. (13) reduces to

$$P_{S_1}(\sigma) = N\cdot\mathbb{P}\{\omega_i^c(\sigma)\}\cdot\prod_{j\neq i}\mathbb{P}\left\{\omega_j(\sigma)\cap\omega_j(\eta_j^{(1)}\sigma)\right\} \tag{15}$$

$$= NP_1(\sigma)\cdot\prod_{j\neq i}\mathbb{P}\left\{\omega_j(\sigma)\cap\omega_j(\eta_j^{(1)}\sigma)\right\} \tag{16}$$

When $\eta_j^{(1)} \geq 1$, the event $\left\{\omega_j(\sigma)\cap\omega_j(\eta_j^{(1)}\sigma)\right\}$ is equivalent to $\omega_j(\eta_j^{(1)}\sigma)$, and when $\eta_j^{(1)} < 1$, this event is equivalent to $\omega_j(\sigma)$. Therefore, the expression for P_{S_1} further reduces to

$$P_{S_1}(\sigma) = NP_1(\sigma)\cdot\prod_{i=1}^{N-1}[1-P_1(\lambda_i\sigma)], \quad \lambda_i = \begin{cases}\eta_i, & \eta_i \geq 1\\ 1, & \eta_i < 1\end{cases} \tag{17}$$

Eq. (17) has been derived without using any knowledge of stress redistribution or any simplifying intuitive assumptions about load sharing rules. To get a simpler estimate of P_{S_1}, we can make two reasonable simplifications of stress redistribution:

1. The stress redistributes only in the vicinity of a failed link. So we assume that links farther away are undisturbed, with all $\eta_i^{(1)} = 1$, and assume the stress to change only a few links, whose number is denoted as ν_1 (not including the failed link);
2. To keep P_f either as an upper bound or an optimum prediction, we replace all the ν_1 redistributed stresses $\eta_i^{(1)}\sigma$ by the maximum $\eta_{max}^{(1)}\sigma$ or by some weighted average $\eta_a^{(1)}\sigma$ among them.

Based on these two additional simplifying assumptions, P_{S_1} is further simplified to:

$$\boxed{P_{S_1}(\sigma) = NP_1(\sigma)[1-P_1(\sigma)]^{N-\nu_1-1}[1-P_1(\eta_a^{(1)}\sigma)]^{\nu_1}} \tag{18}$$

In simple terms, here N means that failure can start in any link, which requires summing the failure probabilities from N mutually exclusive cases. The two bracketed terms mean that the failure of one of the N links must occur jointly with the survival of: (i) each of the remaining $(N-\nu_1-1)$ links with stress σ, and of (ii) each of the remaining ν_1 links with redistributed stress $\eta_a^{(1)}$.

As a reasonable estimate (to be checked by Monte Carlo simulations), we choose ν_1 such that all the $\eta_i^{(1)}$'s that are smaller than 1.1 would be replaced by 1, and then determine the value of $\eta_a^{(1)}$ by approximating Eq. (17) by Eq. (18), i.e.,

$$\prod_{i=1}^{N-1}[1-P_1(\lambda_i\sigma)] \simeq [1-P_1(\sigma)]^{N-\nu_1-1}[1-P_1(\eta_a^{(1)}\sigma)]^{\nu_1} \tag{19}$$

For various strength distributions $P_1(\sigma)$ of the links, we have $\nu_1 = 4\sim 8$ and $\eta_a^{(1)} = 1.34\sim 1.36$. From this, we can see that $\eta_a^{(1)}$ is very close to $\eta_{max}^{(1)}$. This means that using the maximum redistributed stress can actually provide a relatively good prediction of P_f.

To obtain the survival probability, we plug Eq. (18) into Eq. (9):

$$1-P_f(\sigma) = [1-P_1(\sigma)]^N + NP_1(\sigma)[1-P_1(\sigma)]^{N-\nu_1-1}[1-P_1(\eta_a^{(1)}\sigma)]^{\nu_1} \tag{20}$$

$$\text{or} \quad 1-P_f(\sigma)=[1-P_1(\sigma)]^N\left\{1+\frac{NP_1(\sigma)}{1-P_1(\sigma)}\left[\frac{1-P_1(\eta_a^{(1)}\sigma)}{1-P_1(\sigma)}\right]^{\nu_1}\right\} \tag{21}$$

Denoting

$$P_\Delta=\frac{1}{1-P_1(\sigma)}\left[\frac{1-P_1(\eta_a^{(1)}\sigma)}{1-P_1(\sigma)}\right]^{\nu_1} \tag{22}$$

we get an alternative expression

$$1-P_f(\sigma)=[1-P_1(\sigma)]^N\cdot\left\{1+NP_1(\sigma)P_\Delta(\sigma,\eta_a^{(1)},\nu_1)\right\} \tag{23}$$

which reveals that the crucial difference of the two-term fishnet model from the weakest-link model is the extra term:

$$NP_1(\sigma)\cdot P_\Delta \tag{24}$$

In the expression for P_Δ, the bracketed term, i.e., $[(1-P_1(\eta_a^{(1)}\sigma))/(1-P_1(\sigma))]^{\nu_1}$, is the conditional probability of survival for the links in the region of stress redistribution with load ratio $\eta_a^{(1)}\sigma$, given that they have been carrying load σ without failing. In other words,

$$1-\left[\frac{1-P_1(\eta_a^{(1)}\sigma)}{1-P_1(\sigma)}\right]^{\nu_1} \tag{25}$$

takes the form of cumulative distribution function (cdf). Therefore, its survival complement has the following properties:

$$\lim_{\sigma\to 0}\left[\frac{1-P_1(\eta_a^{(1)}\sigma)}{1-P_1(\sigma)}\right]^{\nu_1}=1 \quad \text{and} \quad \lim_{\sigma\to\infty}\left[\frac{1-P_1(\eta_a^{(1)}\sigma)}{1-P_1(\sigma)}\right]^{\nu_1}=0$$

As for the other term in P_Δ, i.e. $1/(1-P_1(\sigma))$, it tends to 1 as σ tends to zero, and blows up as σ approaches ∞. Therefore, as σ tends to 0, the term P_Δ tends to 1. A numerical study of P_Δ shows that, for most cases with P_1 being the Gaussian, Weibull or some grafted distribution, P_Δ always tends to 0 as $\sigma\to\infty$ as long as $\eta_a^{(1)}>\eta_0$, where the constant η_0 depends on P_1 and is greater but very close to 1 (e.g., $\eta_0=1.02$).

For engineering structures such as bridges, aircraft or MEMS, for which $P_f\le 10^{-6}$ is generally required, one obviously needs to pay attention only to the remote left tail of $P_f(\sigma)$, i.e., the tail for $\sigma\to 0$. In that case we have

$$1-P_f(\sigma)\simeq[1-P_1(\sigma)]^N[1+NP_1(\sigma)] \tag{26}$$

To elucidate the difference from the classical weakest-link model, it helps to transform the foregoing equation (Eq. (26)) to the Weibull scale, which has the coordinates:

$$X^*=\ln\sigma,\ \ Y^*=\ln[-\ln(1-P_f)] \tag{27}$$

For comparison, we plot in this scale also the weakest-link model. For $\sigma\to 0$, we have $P_1\to 0$, and so we may think of using the approximation $\ln(1+x)\simeq x$ for small x. However, with this approximation, the logarithm of Eq. (26) gives 0:

$$\ln[1-P_f(\sigma)]\simeq N\ln[1-P_1(\sigma)]+\ln[1+NP_1(\sigma)] \tag{28}$$

$$\simeq -NP_1+NP_1=0 \tag{29}$$

So we must use the second-order approximation $\ln(1+x)\simeq x-x^2/2$. This leads to:

$$\ln[1-P_f(\sigma)]\simeq N\ln[1-P_1(\sigma)]+\ln[1+NP_1(\sigma)] \tag{30}$$

$$\simeq N\left(-P_1-\frac{P_1^2}{2}\right)+NP_1-\frac{(NP_1)^2}{2} \tag{31}$$

$$=-N(N+1)\frac{P_1^2}{2} \tag{32}$$

The previous derivation shows that, by adding the term P_{S_1}, the dominant term of $\ln(1-P_f)$ changed from $P_1(\sigma)$ to $[P_1(\sigma)]^2$, which will be immediately seen to have a huge effect on the left tail of P_f. To obtain the Weibull scale plot, we multiply both sides by -1 and take again the natural logarithm; this yields:

$$Y^*=\ln[-\ln[1-P_f(\sigma)]]=\ln\frac{N(N+1)}{2}+2\ln P_1(\sigma) \tag{33}$$

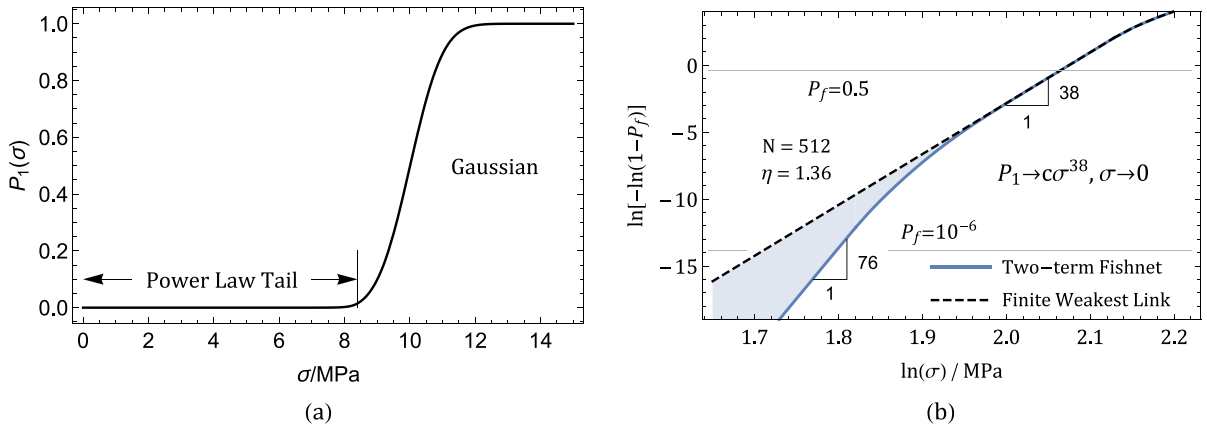

Fig. 6. a) Cumulative distribution function (cdf) of failure for a single truss element; b) Comparison of P_f between finite weakest-link model and fishnet model with 2 terms in expansion (Weibull scale).

For comparison, the Weibull plot for the weakest-link model is

$$Y^* = \ln[-\ln[1 - P_f(\sigma)]] = \ln N + \ln P_1 \tag{34}$$

Since the independent variable of Weibull plot is $X^* = \ln\sigma$, and since $\ln P_1 \simeq \ln(\sigma^m) = m\ln\sigma$, the slope of the Weibull plot for the Weibull distribution is the Weibull modulus m.

Comparing the expressions of Eqs. (33) and (34), one can see that the slope of the far left tail of Weibull plot in the two-term fishnet model got doubled from m to $2m$.

On the other hand, in the region where P_Δ is close to 0, i.e., for large enough σ, Eq. (23) reduces to the weakest-link model. Thus the addition of the term P_{S_1} affects only the far left tail of the cdf of structural strength and has no effect on the right tail. Physically, this is because, when σ_N is very small (far below the mean), the links surrounding the failed link are generally strong enough to bear the redistributed load without breaking. But the weakest-link model characterizes this case as a failure of the whole structure, and this is why it overshoots $P_f(\sigma)$ when the load is small. However, when σ_N is large (far above the mean), the survival probability of the links surrounding the failed one is very small, regardless of the initial failed link. So, on the far right tail, the two-term fishnet model is essentially the same as the weakest-link model.

Fig. 6b shows the difference between the finite weakest-link model and the two-term fishnet model for the case in which $N = 512$, $\eta_a^{(1)} = 1.36$ and $\nu_1 = 6$. The cdf $P_1(\sigma)$ of structure strength is given in Fig. 6a. $P_1(\sigma)$ is considered as the Gaussian (or normal) distribution with a power law tail grafted at cumulative probability $P_1(\sigma) = 0.015$. From Fig. 6b, one should note that the two-term fishnet model exhibits, in the Weibull plot, a smooth transition of slope from $m = 38$ to the doubled slope $2m = 76$. Keep in mind that, since the two-term fishnet statistics does not consider all the terms in Eq. (6), it is still an upper bound for the true $P_f(\sigma)$. Also note that a higher slope m generally implies a weaker size effect (Bažant and Pang, 2006; Bažant and Le, 2017).

The difference between the weakest-link model and the two-term fishnet model in this case is illustrated by the diagram in Fig. 6b. We show two quantitative comparisons. First we fix the load as $\sigma = 6.5$ MPa (drawing a vertical line through $\sigma = 6.5$ MPa) and compare the failure probability P_f obtained with each model; for the fishnet model $P_f = 1.19 \cdot 10^{-6}$, while for the weakest-link model $P_f = 29.5 \cdot 10^{-6}$, which is 24.8 times higher. Second we fix $P_f = 10^{-6}$ and compared the loads; for the fishnet model $\sigma = 5.47$ MPa, while for the weakest-link model $\sigma = 6.05$ MPa, which is 10.5% higher. Hence, the nacreous lamellar architecture provides a significant increase of load capacity for the same safety margin, or a significant decrease of failure risk for the same load.

3.4.3. Location of the slope transition for the 2-term fishnet statistics

It is not enough to know that the left terminal slope in the Weibull plot is doubled. One needs to know also at which σ value the slope transition is centered. According to Eq. (6), this value is controlled by two parameters, $\eta_a^{(1)}$ and ν_1. Here $\eta_a^{(1)}$ is the ratio of the average redistributed stress to the initial uniform stress, and ν_1 is the number of links in the redistribution zone. To study the effects of these two parameters, we fix one of them and plot P_Δ for various values of the other. We consider $N = 512$ and $\nu_1 = 6$. The calculated plots of P_Δ and P_f for $\eta_a^{(1)} = 1.1$, 1.3 and 1.6 are given in Fig. 7.

As the value of P_Δ varies from 0 to 1, the slope of cdf in Weibull scale gradually transits from m to $2m$. Thus the center of the transition is the value σ_T of σ at which $P_\Delta(\sigma_T) = 0.5$. So we set $P_\Delta = 0.5$ for various values of $\eta_a^{(1)}$, and compare the σ_T values. Shown in Fig. 7a, they are seen to match well the kink locations in Fig. 7b. Also note that the kink location shifts dramatically to the left when $\eta_a^{(1)}$ is increased from 1.1 to 1.6. Finally, if $\eta_a^{(1)} \to \infty$, the kink position approaches $\sigma_T = 0$, which means that the fishnet degenerates into the weakest-link model—indeed, as long as one link fails, the stress in its neighborhood becomes infinitely large, and so the structure must fail right after a single link fails.

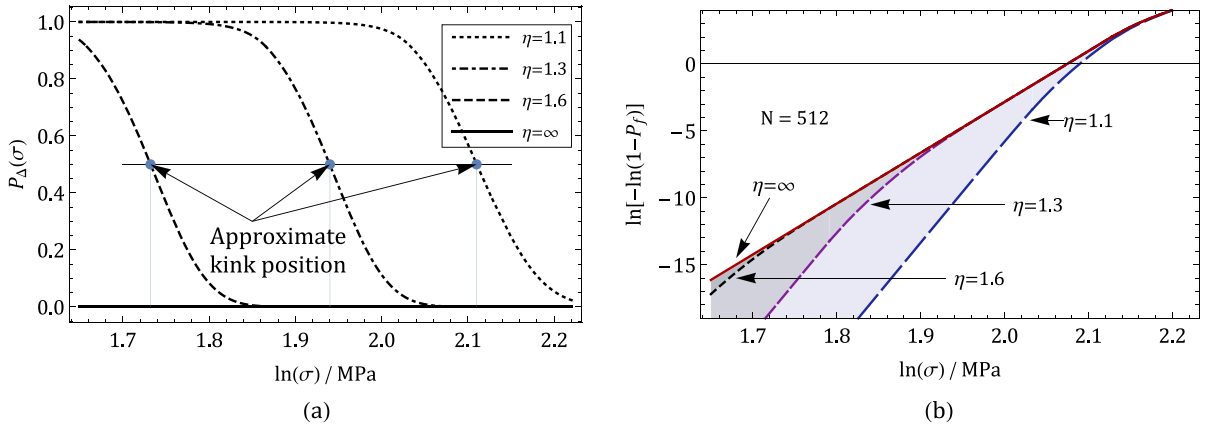

Fig. 7. a) Approximate position of transition for $\eta_a^{(1)} = 1.1$, 1.3 and 1.6; b) Cumulative distribution function (cdf) of $P_f(\sigma)$ in Weibull scale with different $\eta_a^{(1)}$.

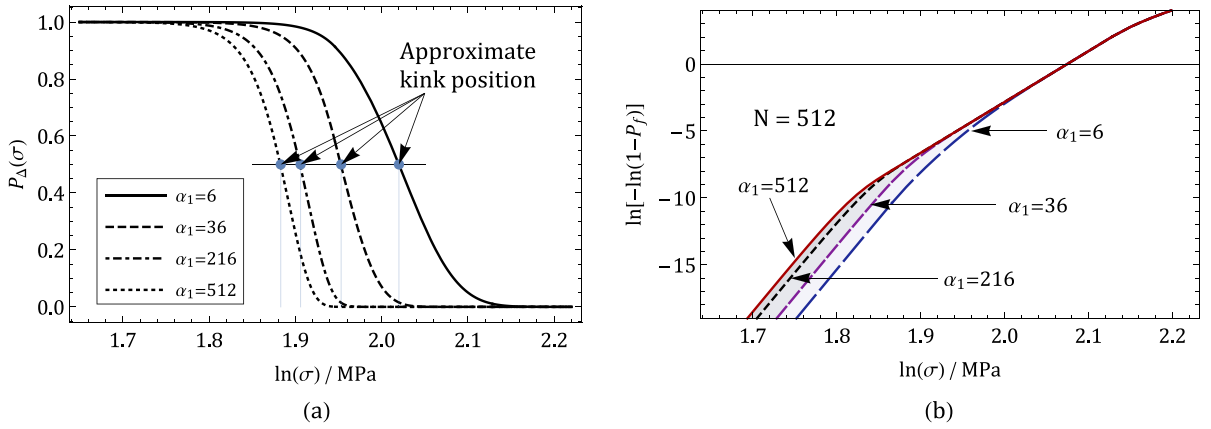

Fig. 8. a) Approximate position of transition for $\nu_1 = 6$, 36, 216 and 512; b) Cumulative distribution function (cdf) of $P_f(\sigma)$ in Weibull scale, for different ν_1.

Next, we fix $\eta_a^{(1)} = 1.2$ and let $\nu_1 = 6$, 36, 216 and 512. Note that, since $N = 512$, the largest ν_1 value cannot exceed 512. Similarly, as ν_1 increases, the kink location shifts to the left (Fig. 8a,b), but the shift is much smaller than the change of $\eta_a^{(1)}$. Thus we conclude that the stress ratio $\eta_a^{(1)}$ has a big effect on the location of slope change from m to $2m$, while ν_1 has a much smaller effect.

3.4.4. Three-term fishnet statistics

To get an even better approximation of P_f, we consider one more term in the sum and keep the first three terms from Eq. (6), i.e., $1 - P_f(\sigma) = P_{S_0}(\sigma) + P_{S_1}(\sigma) + P_{S_2}(\sigma)$. The additional term $P_{S_2}(\sigma)$ is the probability of fishnet survival with two and only two failed links. After the first link fails, the next one to fail will be either a neighboring link or a link located farther away. Since these two events are mutually exclusive, we may write:

$$P_{S_2} = P_{S_{21}} + P_{S_{22}}, \tag{35}$$

where $P_{S_{21}}$ (or $P_{S_{22}}$) is the probability of $\{X(\sigma) = 2\}$ when the failed link is adjacent to (or farther away from) the previously failed link.

Note that the probability density function (pdf) characterizing $P_1(\sigma)$ is $\psi(\sigma) = \mathrm{d}P_1(\sigma)/\mathrm{d}\sigma$, and let ν_2 be the number of links, adjacent to the first failed link, that will endure the redistributed stress after the second link failure. Also, denote the new equivalent redistributed stress ratio as $\eta^{(2)}$ (note that $\eta^{(2)} > \eta_a^{(1)} > 0$).

In both foregoing cases, since there are only 2 failed links (after the original one), we still assume that the stresses in the links far away from the failed ones remain undisturbed and equal the remotely applied stress σ (this ceases to be true when the number of failed links keeps increasing further). Thus we may write:

$$P_{S_{21}} = \binom{N}{1}\binom{\nu_1}{1}\int_0^\sigma \int_{x_1}^{\eta_b^{(1)}\sigma} \psi(x_1)\psi(x_2)dx_2dx_1\ [1 - P_1(\sigma)]^{N-\nu_2-2}\ [1 - P_1(\eta^{(2)}\sigma)]^{\nu_2} \tag{36}$$

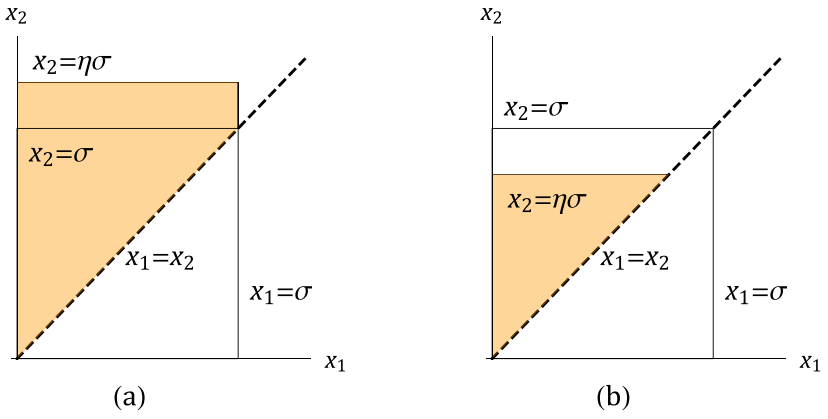

Fig. 9. Domains of integration when (a) $\eta \geq 1$, and (b) $\eta < 1$.

$$P_{S_{22}} = \binom{N}{1}\binom{N-\nu_1-1}{1}\int_0^\sigma \int_{x_1}^\sigma \psi(x_1)\psi(x_2)dx_2dx_1\ [1-P_1(\sigma)]^{N-2\nu_1-2}\ [1-P_1(\eta_a^{(1)}\sigma)]^{2\nu_1} \tag{37}$$

where x_1 and x_2 are the strength of the first and second failed link, respectively, and $\eta_b^{(1)}$ is a parameter calculated from $\eta_i^{(1)}$. This parameter is used by another approximate relation which is similar to, but different from, that for $\eta_a^{(1)}$:

$$\nu_1 \int_0^\sigma \int_{x_1}^{\eta_b^{(1)}\sigma} \psi(x_1)\psi(x_2)dx_2dx_1 \simeq \sum_{j=1}^{\nu_1} \int_0^\sigma \int_{x_1}^{\eta_j^{(1)}\sigma} \psi(x_1)\psi(x_2)dx_2dx_1 \tag{38}$$

Further note that

$$\int_0^\sigma \int_{x_1}^\sigma \psi(x_1)\psi(x_2)dx_2dx_1 = \frac{1}{2}[P_1(\sigma)]^2 \tag{39}$$

Then, according to Fig. 9a,

$$= \int_0^\sigma \int_{x_1}^{\eta_b^{(1)}\sigma} \psi(x_1)\psi(x_2)\mathrm{d}x_2\mathrm{d}x_1 = \int_0^\sigma \int_{x_1}^\sigma \psi(x_1)\psi(x_2)\mathrm{d}x_2\mathrm{d}x_1 + \int_0^\sigma \int_{x_1}^{\eta_b^{(1)}\sigma} \psi(x_1)\psi(x_2)\mathrm{d}x_2\mathrm{d}x_1 \tag{40}$$

$$= \frac{1}{2}[P_1(\sigma)]^2 + P_1(\sigma)[P_1(\eta_b^{(1)}\sigma) - P_1(\sigma)] \tag{41}$$

$$= P_1(\sigma)P_1(\eta_b^{(1)}\sigma) - \frac{1}{2}[P_1(\sigma)]^2 \tag{42}$$

Finally, we obtain

$$P_{S_{21}} = N\nu_1\left\{P_1(\sigma)P_1(\eta_b^{(1)}\sigma) - \frac{1}{2}[P_1(\sigma)]^2\right\}\cdot[1-P_1(\sigma)]^{N-\nu_2-2}\cdot[1-P_1(\eta^{(2)}\sigma)]^{\nu_2} \tag{43}$$

$$P_{S_{22}} = \frac{1}{2}N(N-\nu_1-1)[P_1(\sigma)]^2\cdot[1-P_1(\sigma)]^{N-2\nu_1-2}\cdot[1-P_1(\eta^{(2)}\sigma)]^{2\nu_1} \tag{44}$$

So, considering three terms in Eq. (6), we find the three-term failure probability of fishnet to be

$$1-P_f(\sigma) \simeq [1-P_1(\sigma)]^N\cdot\left\{1+P_{S_1}/[1-P_1(\sigma)]^N + P_{S_2}/[1-P_1(\sigma)]^N\right\} \tag{45}$$

$$= [1-P_1(\sigma)]^N\cdot\left\{1+NP_1(\sigma)P_\Delta + N\nu_2\left[P_1(\sigma)P_1(\eta_b^{(1)}\sigma) - \frac{1}{2}[P_1(\sigma)]^2\right]P_{\Delta_{21}}\right. \tag{46}$$

$$\left. + \frac{1}{2}N(N-\nu_1-1)[P_1(\sigma)]^2P_{\Delta_{22}}\right\},$$

where

$$P_\Delta = \frac{[1-P_1(\eta_a^{(1)}\sigma)]^{\nu_1}}{[1-P_1(\sigma)]^{\nu_1+1}},\quad P_{\Delta_{21}} = \frac{[1-P_1(\eta^{(2)}\sigma)]^{\nu_2}}{[1-P_1(\sigma)]^{\nu_2+2}},\quad P_{\Delta_{22}} = \frac{[1-P_1(\eta_a^{(1)}\sigma)]^{2\nu_1}}{[1-P_1(\sigma)]^{2\nu_1+2}} \tag{47}$$

Similar to P_Δ, $\lim_{\sigma\to 0} P_{\Delta_{21}} = 1$ and $\lim_{\sigma\to 0} P_{\Delta_{22}} = 1$.

For intuitive understanding of Eq. (46), note that the multipliers N and $(N-\nu_1-1)$, which are the values of combinatorial coefficients $\binom{n}{1}$ and $\binom{N-\nu_1-1}{1}$ ensue from the fact that, for the first and second link failures, there are N and ν_1 or $N-\nu_1-1$ mutually exclusive possibilities. The integrals over the pdf of P_1 in Eq. (40) express the joint probability of two links failing, the second integral at higher stress than the first one (which translates into the restriction $x_2 \geq x_1$ giving the triangular domain in Fig. 9). The bracketed terms give the condition of simultaneous survival of the remaining links, both those with and without the elevated redistributed stress. The term $\frac{1}{2}{P_1}^2(\sigma)$ ensues from integrating over a triangular domain in plane (x_1, x_2) bordered by line $x_2 = x_1$ (Fig. 9).

Note that the foregoing expression for P_{S_2} gives only an approximate estimate of the three-term failure probability because we simplified, in two steps, the stress redistribution as a uniform scaling of the stress by factors $\eta_b^{(1)}$ and $\eta^{(2)}$. These factors are both greater than 1. In reality, however, near the group of failed links there are also shielded regions which undergo unloading and have stress smaller than the remotely applied stress σ. The failure probability of these regions is the integral of joint probability density over the domain shown in Fig. 9b. This integral would make a more accurate solution since stronger links can fail prior to the weaker ones if unloading happens in the weak links. Nevertheless, our estimation can still be quite accurate if the uniform factor $\eta_b^{(1)}$ is chosen judiciously, based on Eq. (38).

Since the probability P_{S_2} consists of two terms, namely $P_{S_{21}}$ and $P_{S_{22}}$, another interesting question arises: Which one of these two terms is larger? Eqs. (36) and (37) tell us that $P_{S_{21}}$ is proportional to $N[P_1(\sigma)]^2$, while $P_{S_{22}}$ is proportional to $N(N-\nu_1-1)[P_1(\sigma)]^2$, which approximately equals $N^2[P_1(\sigma)]^2$. Therefore, $P_{S_{22}}$ is much larger than $P_{S_{21}}$. This means that the second link failure will most likely appear far away from the first one if the left tail of $P_1(\sigma)$ is relatively heavy such that the effect of $[P_1(\sigma)]^2$ would still be recognizable. This tendency to scattered damage will be discussed later.

3.4.5. Ramifications to higher-order terms in failure probability

Intuitively, P_{S_r} is proportional to $[P_1(\sigma)]^r$ when σ is close to 0, and so Eq. (6) is similar to a Taylor series expansion of some real function in terms of $P_1(\sigma)$. The higher the order, the smaller the contribution to the total sum. If the tail of $P_1(\sigma)$ is very light, $[P_1(\sigma)]^r$ for $r \geq 3$ are usually too small to be seen on the cdf directly. So, in order to see the effect of the higher-order terms, we need, once again, to study them in the Weibull scale. This scale exponentially magnifies tiny differences in the tail of a distribution.

What will happen if we include more and more terms on the right-hand side of Eq. (6)? Will they cause further slope increases in the Weibull plot? The answer is affirmative: The higher-order terms of survival probability could lead to a further slope increase of cdf in the Weibull scale. From the derivation of Eq. (30), we know that the prime reason for the slope increase by the factor of 2 is that the term $P_1(\sigma)$ got essentially wiped out by the Taylor series expansion, allowing $[P_1(\sigma)]^2$ to dominate. So, if there is another slope increase from $2m$ to $3m$, the squared terms $[P_1(\sigma)]^2$ in Eq. (30) would have to vanish after adding more terms of P_{S_r} in Eq. (6).

To show that the lower-left slope of cdf in Weibull scale could further increase due to the presence of more terms in the expansion of survival probability, we would have to use the exact stress redistribution law, or else we could arrive at false conclusions. However, this law is almost impossible to obtain analytically.

Therefore, instead of working on a general fishnet, it is much easier to consider the limiting special form, i.e., the fiber bundle. By changing the aspect ratio k:n gradually to N:1, a fishnet with a fixed number of links reduces to a fiber bundle. Then one can use the law of stress redistribution in a fiber bundle, to calculate the slope change of the cdf. However, the case of general fishnet is better studied numerically, by Monte Carlo simulations, as discussed later.

Next we consider a fiber bundle consisting of N fibers, and truncate Eq. (6) at P_{S_2}. Consequently, the terms P_{S_0}, P_{S_1} and P_{S_2} can be expressed as:

$$P_{S_0} = [1 - P_1(\sigma)]^N \tag{48}$$

$$P_{S_1} = NP_1(\sigma)\left[1 - P_1\left(\frac{N\sigma}{N-1}\right)\right]^{N-1} \tag{49}$$

$$P_{S_2} = N(N-1)\int_0^\sigma \int_0^{N\sigma/(N-1)} \psi(x_1)\psi(x_2)dx_2dx_1 \cdot \left[1 - P_1\left(\frac{N\sigma}{N-2}\right)\right]^{N-2} \tag{50}$$

Then, as before,

$$\int_0^\sigma \int_0^{N\sigma/(N-1)} \psi(x_1)\psi(x_2)dx_2dx_1 = P_1(\sigma)P_1[N\sigma/(N-1)] - \frac{1}{2}[P_1(\sigma)]^2 \tag{51}$$

Therefore,

$$P_{S_2} = N(N-1)\left\{P_1(\sigma)P_1[N\sigma/(N-1)] - \frac{1}{2}[P_1(\sigma)]^2\right\}\left[1 - P_1\left(\frac{N\sigma}{N-2}\right)\right]^{N-2} \tag{52}$$

The probability of survival of the whole fishnet can then be expressed as:

$$1 - P_f(\sigma) \simeq P_{S_0} + P_{S_1} + P_{S_2} \tag{53}$$

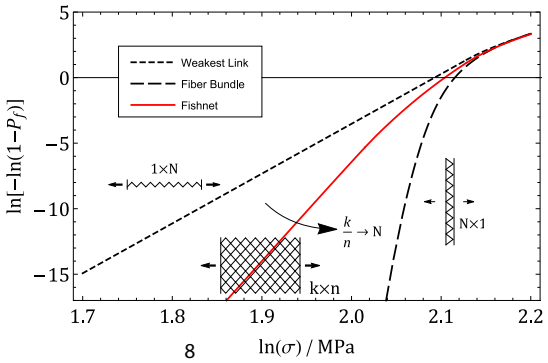

Fig. 10. Change of failure probability of a rectangular fishnet caused by changing the aspect ratio k/n gradually from 1: N to N: 1 at constant number of links.

Now we can factor out $[1-P_1(\sigma)]^N$ and let $\sigma \to 0$:

$$1-P_f(\sigma) \simeq [1-P_1(\sigma)]^N \cdot \left\{1+NP_1(\sigma)+N(N-1)P_1(\sigma)P_1[N\sigma/(N-1)]-\frac{N(N-1)}{2}[P_1(\sigma)]^2\right\} \tag{54}$$

By the same procedure, we now take the natural log of both sides, apply the Taylor series expansion of $\log(1+x)$, and collect all the terms of order smaller than $[P_1(\sigma)]^3$:

$$\log[1-P_f(\sigma)] \simeq -NP_1(\sigma)-\frac{N}{2}[P_1(\sigma)]^2+NP_1(\sigma)-\frac{N^2}{2}[P_1(\sigma)]^2 \tag{55}$$

$$-\frac{N(N-1)}{2}[P_1(\sigma)]^2+N(N-1)P_1(\sigma)P_1[N\sigma/(N-1)] \tag{56}$$

$$=-N^2P_1(\sigma)\left[P_1(\sigma)-\frac{N-1}{N}P_1\left(\frac{N\sigma}{N-1}\right)\right]\to 0 \text{ as } N\to\infty \tag{57}$$

We can now see that considering the term P_{S_2} in Eq. (6) could make all the first and second order terms of $\log[1-P_f(\sigma)]$ vanish. This means that $[P_1(\sigma)]^3$ dominates when σ is small enough. Therefore the left asymptotic slope of the cdf of fishnet strength in the Weibull scale increases by the factor of 3.

3.4.6. Upper and lower bounds on failure probability of fishnet

As already became clear, a rectangular fishnet possesses two geometrical limits—the (weakest-link) chain and the fiber bundle. It reduces to a chain for the aspect ratio $k{:}n\to 1{:}N$, and to a fiber bundle for $k{:}n\to N{:}1$ (the tensile load in Fig. 10 is assumed to be applied horizontally). Intuitively, given the same amount of links, a fiber bundle would be much more reliable than a single chain: failure of one link will not necessarily lead to rupture of the whole bundle.

Therefore, we conjecture that the upper and lower bounds of the cdf of a fishnet should be those of the weakest-link and the fiber bundle consisting of the *same* number (N) of links, respectively (see Fig. 10). Furthermore, if $P_f(\sigma)$ is assumed to change continuously and monotonically, the fishnet gradually transforms from a chain to a bundle. The failure probability decreases when the aspect ratio k/n increases at a fixed value of the product $k\times n=N$.

4. Large-scale monte carlo simulations of fishnet failure

4.1. Setup of finite element model

To verify the theory, numerical Monte Carlo experiments are conducted by finite element (RE) simulations (in Matlab). In the FE model, the size of a rectangular fishnet is defined by its number of rows and columns, $k\times n$. Each link is treated as an elastic truss element. All the elements (or links) have the same cross section area and Young's modulus, and differ only in their strength, s_i, which is a random variable that follows the probability distribution $P_1(\sigma)$. Concerning real nacre, the randomness of link strength approximately replaces the random scatter in the length and overlap of the lamellae.

The nodes at the left fishnet boundary are fixed in x direction but allowed to slide freely in the transverse y direction. The fishnet is loaded under displacement control. The tensile load is applied by prescribing increments of a uniform displacement u_0 at the right boundary nodes while allowing free transverse sliding.

4.2. Random variable generation

Random variables s_i are generated by the inverse-transform method. First, we use the random number generator in Matlab to generate random variables x_i in the interval [0, 1], and then apply the inverse of P_1 to each x_i, i.e. $s_i = P_1^{-1}(x_i)$. Based on previous research (Le et al., 2011), $P_1(s)$ is defined by grafting a power-law left tail onto a Gaussian distribution.

The grafting point probability, P_g, needs to be determined empirically and, similar to concrete, size effect test would be most effective for that purpose. P_g is probably much higher than 0.001, the value previously identified from the size effect tests of quasibrittle materials such as concrete, tough ceramics and fiber composites (Bažant and Le, 2009; 2017; Bažant et al., 2009; Le et al., 2011). The reason is that the link failure in nacre actually represents an interface shear fracture (with some bending) in a thin and long bio-polymer layer that binds parallel lamellae together. This layer is, in itself, a structure failing only after a sizable shear fracture process zone with a certain characteristic length develops. In analogy to the previous analysis (Bažant and Le, 2017; Le and Bažant, 2010) of shear failure and size effect of laminate-steel interfaces, this zone may have a significant characteristic length producing quasibrittle behavior, for which a Gauss-Weibull cdf with a grafting point at higher P_f values may be expected. Hence we will consider P_1 with a grafting point P_g up to about 0.3.

The stiffnesses of links (EA/l_e) are not treated here as random variables. This is not a major simplification. To explain why not, consider a $k \times n$ fishnet with i.i.d. random stiffnesses $K_{i,j}$ for the individual links. Now, if the x-displacement at left boundary is zero and at the right boundary is nu_0, then the elongation of each link is u_0. So, if we pick any cross-section, the total force and nominal stress are:

$$P = u_0 \sum_{l=1}^{k} K_l, \quad \sigma_N = \frac{u_0}{A}\left(\frac{1}{k}\sum_{l=1}^{k} K_l\right) \tag{58}$$

where K_l is the element stiffness of the l-th link along the picked cross-section of fishnet, and A is the element cross-section area. This means that the random variable σ_N is proportional to the sample mean of K_l. According to the weak law of large numbers, the sample mean converges to the true mean with probability 1 as $k \to \infty$. Intuitively, this means that, given any form of the distribution of $K_{i,j}$, the nominal stress σ_N always follows the law of a degenerate Gaussian distribution, i.e., the Dirac Delta function, centered at $\sigma_N = Ku_0/A$ if the cross-section contains a sufficiently large number of elements, where K is the mean of all K_l.

Therefore, no matter what the distribution is for the stiffness of a single element, its influence on the randomness of nominal strength is negligible. This is also true if the fishnet is slightly damaged, because we can always find a cross-section that is sufficiently far away from the zone of failed links. Indeed, the elongation of these elements on the chosen cross-section is still approximately u_0, which means that Eq. (58) still holds. Therefore, it suffices to randomize the strength of each link while considering the element length, elastic modulus and cross-section area as deterministic.

4.3. Element deletion and propagation of cracks

The time steps are indexed by the total number (τ) of failed links. At the beginning of time step τ, we set $u_0 = 1$ and calculate the stresses of each element $\sigma_j^{(\tau)}$. Then the only element, indexed by i, that is going to fail in this new time step, is the one whose stress satisfies the condition:

$$\lambda^{(\tau)} = s_i/\sigma_i^{(\tau)} = \min_j \{s_j/\sigma_j^{(\tau)}\} \tag{59}$$

where s_j is the strength of the jth element. Since the constitutive law is linear elastic, $\lambda^{(\tau)}$ is the load multiplier such that, if we reset $u_0 = \lambda^{(\tau)}$ and recalculate the stress field, we will have $\sigma_i^{(\tau)} = s_i$ and $\sigma_j^{(\tau)} < s_j$ for $i \neq j$.

So the final stress state of each element at the current time step is calculated by $\sigma_{j_{\text{new}}}^{(\tau)} = \lambda\ \sigma_i^{(\tau)}$. After updating the stresses, the critical ith element is deleted, and its element stiffness matrix $\boldsymbol{K}_{ei}^{(\tau)}$ will not be assembled into the global stiffness matrix $\boldsymbol{K}^{(\tau)}$ for future loading steps. The element deletion is equivalent to unloading the fishnet to the origin and immediately reloading it with the modified stiffness matrix. This process keeps repeating until the global stiffness matrix becomes singular, which means that a contiguous crack has already gone through the whole cross-section and the fishnet load dropped to zero.

In nacre, the deletion of links is equivalent to a sudden drop of shear transmission through the biopolymer layer binding the adjacent lamellae. Progressive softening of the links might, of course, be closer to reality. But in the sense of the crack band model (Bažant and Planas, 1998), progressive softening for one spacing of fishnet nodes should be approximately equivalent to a sudden stress drop in a fishnet with a certain enlarged spacing of nodes. In this sense, despite sudden stress drop, the fishnet model with a reduced number of nodes should give an approximately correct overall representation of the failure of nacre.

Indexing the time steps by the number of failed links allows us to obtain not only the peak load but also the complete load-displacement curve, without worrying about stability issues. As it turns out, the load-displacement curve of an elastic fishnet with a sudden stress drop in the links may give, for a sufficiently large fishnet size, a strong snap-back instability, as exemplified later.

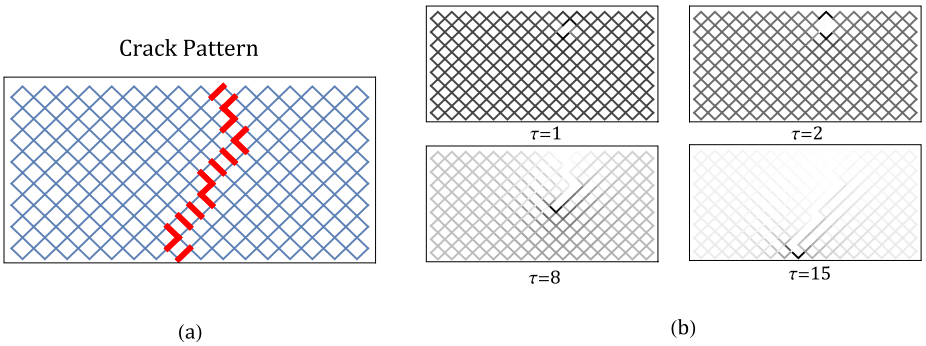

Fig. 11. a) Crack pattern of a 16×32 fishnet with random link strength of a rather low CoV = 0.078%, with grafting probability $P_g = 0.015$, and (on the right) the corresponding crack patterns (b) Stress evolution as crack propagates through the fishnet (the darker the lines, the larger the relative stress σ/σ_{max}), where τ is the number of failed links.

4.4. Results of finite element (FE) simulations

Fig. 11a shows the load-displacement curve obtained in FE simulation of 16×32 fishnets with random link strengths. The distribution of random strength is a Gaussian distribution $N \sim (10,\ 0.4^2)$ grafted with a power law tail at $P_1(\sigma) = 0.015$. For a small enough coefficient of variation (CoV) of link strength, with peaking of the load and a strong snap-back instability of a fishnet with an initial failed link, instability occurs right after the rupture of the first link. If there is no randomness in strength (CoV = 0), the fishnet will reach the maximum load and fail as soon as any one of the links succumbs. Thus, a deterministic fishnet exhibits the Type I failure (Bažant and Le, 2017).

This observation confirms that it is the strength randomness that makes it possible for the whole structure to survive the failure of a few links. In a more detailed representation of nacreous materials, the nodes would not act locally as pin nodes and would resist bending moments, which would generally cause the maximum load to be preceded by the failure of more links, or shear connections. This would be similar to the type I failure in brittle heterogenous materials, in which several microcracks between grains must form in a representative volume element (RVE) before a macrocrack propagation from the RVE is initiated.

Fig. 11b illustrates the stress field of 4 typical fishnet frames ($\tau = 1,\ 2,\ 8,\ 15$) in the process of crack propagation. In this particular case, subsequent link failures localize immediately after the crack initiation, and no scattered damage is observed. One can see that the random crack path in this case has a clear tendency to extend, after the peak load, transversely, to form a full break. Another observation is that, as the crack propagates, the darkness contrast in the figures gradually increases, which means that the difference between maximum stress σ_{max} and nominal stress σ_N becomes larger and larger.

4.5. Verification of fishnet theory

Millions of finite element simulations with random inputs are run to verify the fishnet statistics. The criterion of convergence is set as follows: First we consider the curve of the estimated distribution obtained from many runs of fishnet samples of size n_1 in Weibull scale. Then we increase the sample size n_1 by one, and consider the curve of the newly estimated distribution. The part of the curve that does not change appreciably upon doubling the sample size is considered as converged (for example, one plots the estimated distribution in Weibull scale with 1000 and 2000 data points, respectively, and the part of curve for which both distributions are the same can be treated as converged).

To obtain an accurate estimate of the distribution, especially in its left tail, at least one million (10^6) random samples, for each case, have been generated and simulated by FE. Based on such scenario, the distribution estimated from the histogram of the results of all computer runs converges very well to the exact distribution in the region $Y = \ln[-\ln(1-P_f)] > -10$, as seen in the Weibull scale. This corresponds to the interval $4.54 \times 10^{-5} \le P_f < 1$.

4.5.1. Two-term fishnet model

When $P_1(\sigma)$ is a Gaussian $N(10,\ 0.8^2)$ grafted with a power law tail at $P_f = 0.015$, its tail is relatively light and the two-term fishnet model works very well. The expression of $P_1(\sigma)$ is chosen as

$$P_1(\sigma) = \begin{cases} 0.11338 \cdot (\sigma/10)^{38}, & \sigma \le 8.4 \text{ MPa} \\ 0.015 + \{0.481 - 0.504 \cdot \text{erf}[0.884(10-x)]\}, & \sigma > 8.4 \text{ MPa} \end{cases} \tag{60}$$

where

$$\text{erf}(x) = \frac{2}{\sqrt{\pi}} \int_x^{\infty} e^{-t^2} dt. \tag{61}$$

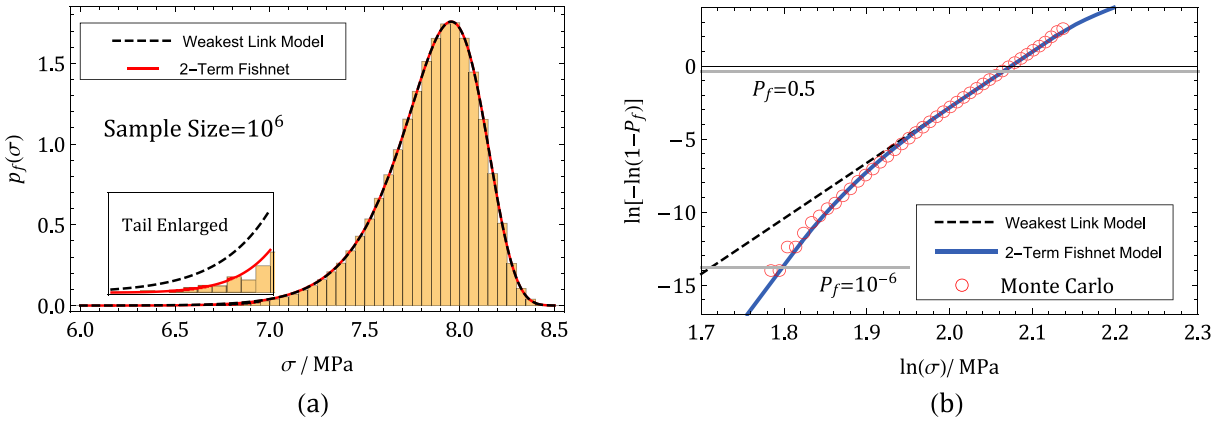

Fig. 12. (a) Histogram of Monte Carlo Experiment of 10^6 samples (the frequency is normalized to probability density) on 16×32 fishnets compared with the density functions of the weakest-link model and 2-term fishnet model; (b) The same data converted into cumulative probability distribution and plotted in the Weibull scale.

Fig. 12a shows the estimated pdf, $p_f(\sigma) = \mathrm{d}P_f(\sigma)/\mathrm{d}\sigma$, obtained from the histogram of Monte Carlo simulations, and compares this pdf with the prediction of the weakest-link model (black dashed line) and of the two-term fishnet model (continuous line). These two predictions are almost indistinguishable in the range $\sigma > 6.7$ MPa and match very well the Monte Carlo experiments. However the difference shows up in the tail ($\sigma \leq 6.7$ MPa). Obviously, the two-term fishnet model fits the Monte Carlo data much better than the classical weakest-link model. The difference is more obvious when it is plotted in Weibull scale; see Fig. 12b: the results of Monte Carlo simulations match the two-term fishnet model everywhere in the figure, while the weakest-link model works well only in the range $\ln\sigma > 1.9$.

4.5.2. Three-term fishnet model

The effect of P_{S_2} in Eq. (6) becomes more significant if the tail of $P_1(\sigma)$ gets heavier. Now consider the case where $P_1(\sigma)$ is a grafted distribution of Gaussian $N(10, 0.8^2)$ and of a power law tail with the grafting point $P_f(\sigma) = 0.08955$:

$$P_1(\sigma) = \begin{cases} 2.551 \cdot \left[1 - e^{-(\sigma/12)^{10}}\right], & \sigma \leq 8.6 \text{ MPa} \\ 0.08955 + \{0.436 - 0.474 \cdot \mathrm{erf}[0.884(10 - x)]\}, & \sigma > 8.6 \text{ MPa} \end{cases} \tag{62}$$

The location of the grafting point is physically determined by the failure mode of the thin polymeric layers bonding the parallel lamella in nacre. Similar to a previous study of size effect in shear bond between laminates and steel (Bažant and Le, 2017; Hoover and Bažant, 2014), the bond layer is itself a substructure in which the shear damage within a portion of the layer causes failure of the whole. So, one must expect that the grafting point of the Gauss-Weibull distribution is already pushed significantly into the Gaussian core. Therefore it is likely that P_1 of one link at the grafting point is much closer to the mean than 0.001, the typical values for particulate quasibrittle materials.

To see the effect on the left tail "thickness", i.e., of the extent of the power-law tail, we calculate that, for $\sigma = 6.7$ MPa, a change of the grafting point from $P_1(\sigma) = 0.1\%$ to $P_1(\sigma) = 9\%$ increases P_1 from 2.79×10^{-6} to 7.5×10^{-3}. This increase makes the tail much "thicker" than in the previous case. Once again, for this particular strength distribution $P_1(\sigma)$ of a single element, and for the 16×32 fishnet, one million samples of Monte Carlo simulations have been obtained.

Fig. 13 shows the estimated density function of P_f with $P_1(\sigma)$ as mentioned above and its comparison with the predictions of the weakest-link model, 2-term (Eq. (23)) and 3-term (Eq. (43)) fishnet model. We can see that the weakest-link model gives a poor prediction of failure probability, while the fishnet models are much better. Note that, as more and more terms of P_{S_r} are considered in the fishnet model, the skewness of the corresponding distribution becomes smaller and smaller. From Fig. 13(b), all of the three predictions are upper bounds of the true failure probability, as expected. When σ decreases, the Monte Carlo results begin to deviate from the two-term fishnet model and a further slope increase is observed.

Apart from the Monte Carlo results of the structures strength σ_{max} (shown by circle points), the histogram of results ($\sigma_{max}^{(1)}$ and $\sigma_{max}^{(2)}$) that exclude the events with more than 1, or more than 2, failed links, respectively, are shown by triangles and squares in Fig. 13b. As we see, the results agree very well with the analytical two-term and three-term fishnet models. The three-term fishnet model gives the better prediction. To get a still more accurate prediction, we would need to consider the next term, P_{S_3}, or even more terms, in the expansion of Eq. (6).

4.5.3. Scattered damage versus localized damage

The previous Monte Carlo simulations show that changing the tail of strength distribution of a single link could have a huge effect on the failure probability of the whole structure. To explain it intuitively, we run finite element simulations for a

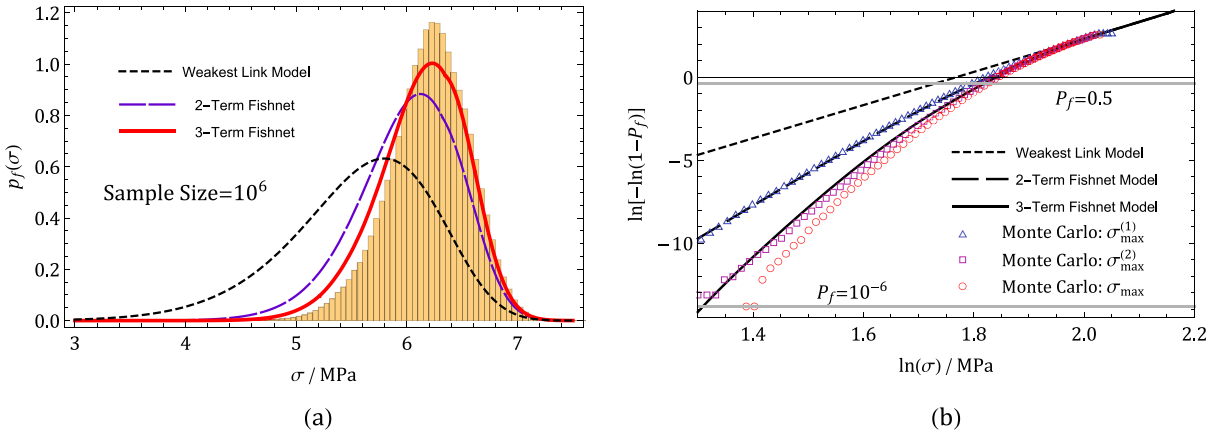

Fig. 13. (a) Histogram of Monte Carlo experiment (σ_{max}) of 10^6 samples (frequency being normalized to probability density) compared with the probability density functions of weakest-link model, 2-term and 3-term fishnet model; (b) The same data as well as the Monte Carlo results of $\sigma^{(1)}_{max}$ and $\sigma^{(2)}_{max}$ converted into cumulative probability distribution and plotted in Weibull scale.

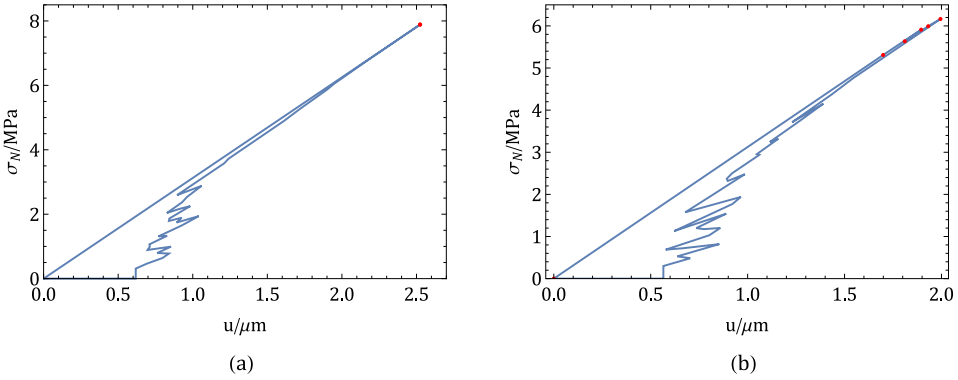

Fig. 14. Load-displacement curve of a horizontally pulled 32×32 square fishnet in which the strength distribution of a single link a) P_1 has a thin power law tail, with $P_g = 0.015$; b) P_1^* has a thick Weibull tail, with $P_g = 0.08955$ (damages before the prepeak are marked with dark points).

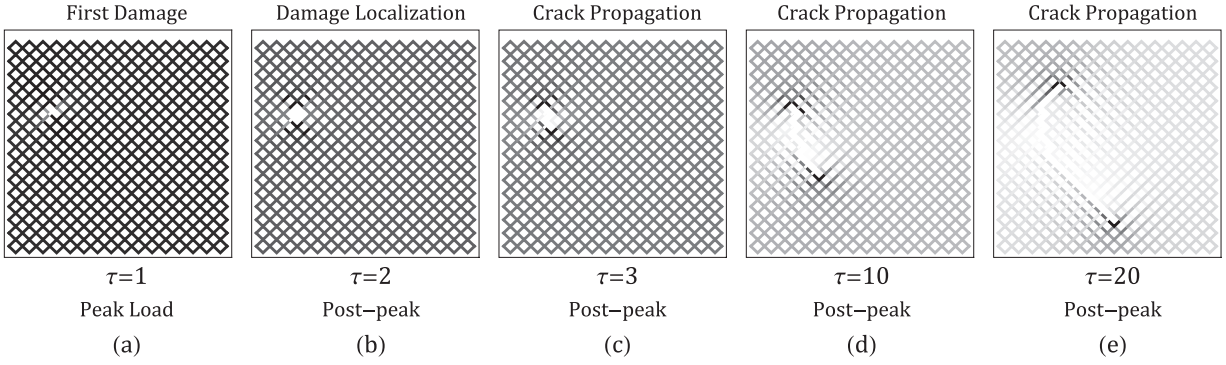

Fig. 15. Stress evolution in a 32×32 square fishnet whose strength distribution of a single link is P_1, which has a thin power law tail. In each figure, the stress is normalized by the maximum σ^{τ}_{max} of that moment. Pure black corresponds to σ^{τ}_{max} and pure white corresponds to zero stress.

32×32 square fishnet for two different strength distributions of a single link $P_1(\sigma)$ and $P_1^*(\sigma)$, where $P_1(\sigma)$ is the Gaussian distribution grafted with a light power law tail (Eq. (60)) and $P_1^*(\sigma)$ is the one with a heavy Weibull tail (Eq. (62)). Their CoV's are 0.078 and 0.1.

First, consider the case of $P_1(\sigma)$. A typical simulation result is shown in Fig. 15a–e whose curve of load versus load-point displacement curve is shown in Fig. 14a. Due to the fact that $P_1(\sigma)$ has a very thin power law tail, the probability that there exists an extremely weak link is vanishingly small. Therefore, in most cases, the peak load is reached right before the first rupture. Then the successive failures localize and form a single crack. This means that, with a very high probability, the

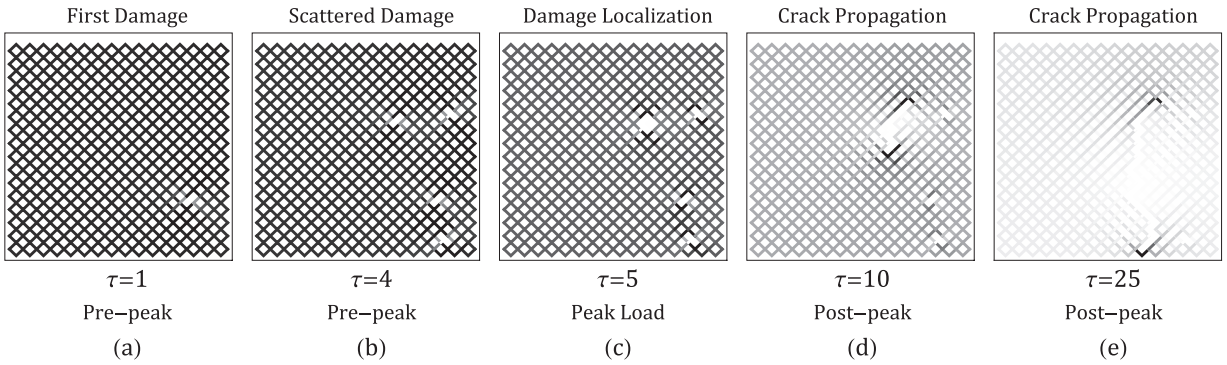

Fig. 16. Stress evolution of a horizontally pulled 32×32 square fishnet in which the strength distribution, P_1^*, of a single link has a thick Weibull tail. In each figure, the stress is normalized by the maximum σ_{max}^{τ} reached at that moment. Perfect black corresponds to σ_{max}^{τ} and perfect white corresponds to zero stress.

failure of structure is the result of rupture of a single link. Then the weakest-link model predicts the P_f quite accurately, as long as σ is not too small.

The scenario gets more complicated as the tail of P_1 becomes thicker. Very likely, a few fishnet links have very low strengths, and their failures will affect the fishnet strength very little. Moreover, these very weak links are scattered through the whole fishnet. As the loading of fishnet begins, these weakest-elements will fail successively at very small nominal stresses, while the rest of the "normal" links are still safe and sound.

As long as the first few damages are scattered, the stress field will keep to be almost uniform except near these failed links. In this case, the failure of one or two links need not lead to the failure of the whole structure, and neither the weakest-link model nor the two-term fishnet model can give good estimates of P_f. This is why we need to consider more higher-order terms in the formula Eq. (6) of survival probability.

Fig. 16a–e, shows the typical pattern of stress evolution when the link strength distribution, $P_1^*(\sigma)$, has a thicker Weibull tail and its load-displacement curve is shown in Fig. 14b. In this particular case, the damage zone does not localize until the fifth rupture, occurring just after the peak load is reached. Once the damages start to localize, the stress concentration at the crack front will only get higher and higher, making the rest of the links bear smaller and smaller stresses and the next failures more likely to localize.

Consequently, the nominal stress keeps decreasing. In this process, damage localization offers a positive feedback to the system: the current localization leads to a higher stress concentration, making the next failure more likely to localize. This process starts when σ_{max} is reached, at which moment stability would get lost if the load were controlled. The peak load occurs right at the moment of damage localization. This moment depends strongly on the "heaviness" of the tail of $P_1(\sigma)$.

4.5.4. Shape effect: transition from chain to bundle

The fact that the peak load is most likely reached at the onset of damage localization helps to decide how many terms of P_{S_r} are needed to get an accurate enough prediction of P_f. For a given $P_1(\sigma)$ of strength distribution of one link and for a given size and shape of fishnet, the approximate number of terms we need to add in the fishnet model should be greater than the average number of scattered failures before localization. The more terms get added, the more accurate the estimation in the tail of P_f will be.

The terms corresponding to link failures after peak load should not be counted, although they are usually negligible.

It thus becomes clear that the fiber bundle must give the lower bound on the strength of all fishnets consisting of the same number of links. The fiber bundle has the largest cross section, and no stress concentration. So the stability limit of a bundle is reached the latest and each term P_{S_r} is the largest among all fishnets. Therefore we have to consider most terms P_{S_r} in the expansion of survival probability Eq. (6) so as to get an accurate estimation of P_f. Hence, the survival probability, $1 - P_f$, of a bundle is the upper bound for those of all fishnets and, accordingly, the failure probability, P_f, of a bundle is the lower bound on all the failure probabilities of all fishnets.

Fig. 17 shows the transition of failure probability P_f of fishnets of various aspect ratios, consisting of the same number, N, of links. The circles with different colors correspond to results of Monte Carlo simulations. Since we want to verify only the qualitative effect of aspect ratio on P_f, we reduce the sample size from 10^6 to 2×10^5. Accordingly, we focus only on the range $\ln[-\ln(1 - P_f)] \geq -6$, in which the histogram has converged quite close to the true distribution.

As shown in the figure, the weakest-link model (dashed line) is the strict upper bound for all fishnets with the same number of links, and the fiber bundle (dashed line) is the strict lower bound. When the fishnet is long and thin, for example $k \times n = 2 \times 128$ (dark small circles), the corresponding P_f can be described quite well by the two-term fishnet model, which shows a gradual slope increase by a factor of 2 as $\sigma_N = \sigma$ tends to 0.

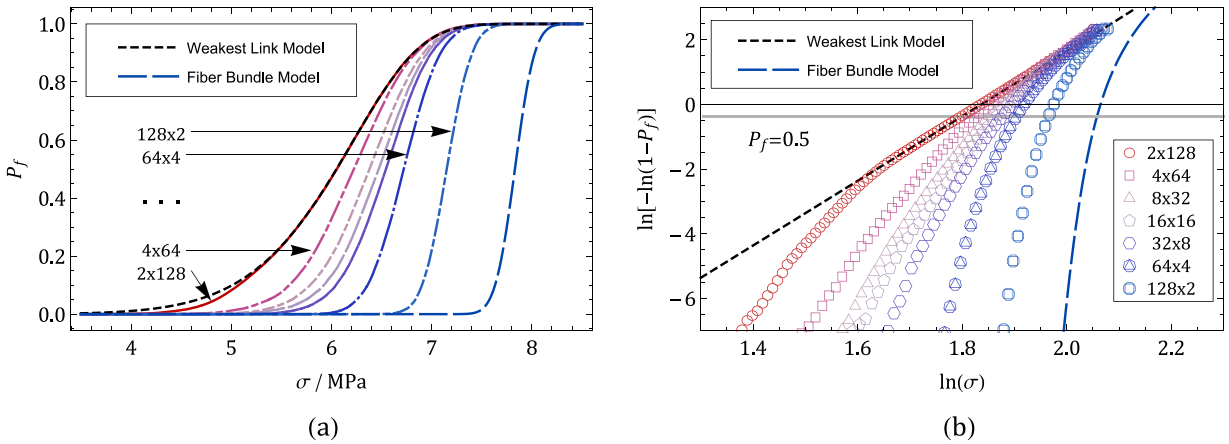

Fig. 17. a) Monte Carlo simulations showing the transition of P_f as the aspect ratio of fishnet is changed from $1 \times N$ to $N \times 1$ ($N = 256$); b) The same data plotted in Weibull scale.

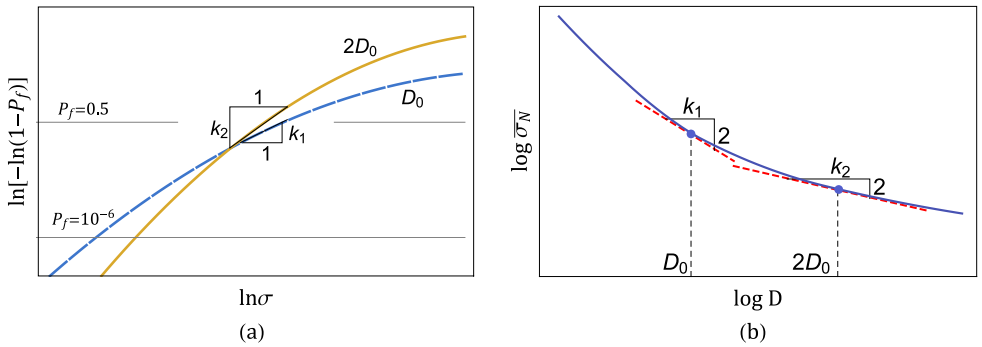

Fig. 18. a) Schematic illustration of P_f for two square fishnets with $D = D_0$ and $D = 2D_0$; b) The corresponding size effect curve.

The case of a uniformly stressed, long and narrow, fishnet cannot be described adequately by the two-term fishnet model, because this model applies if only one additional link fails before the maximum load. The higher-order terms in the expansion of P_f matter. Although they are hard to calculate analytically, insight can be gained by Monte Carlo simulations.

Further we run simulations for fishnets of sizes 64×16 and 16×64, and then count the average number, r_p, of scattered link failures before the peak load is reached (the distribution of r_p should in fact lead to the Poisson distribution with rate parameter μ_p when total number of links $N \to \infty$). For fishnets of size 64×16, $\mu_p \simeq 5.2$, while, for fishnets of size 16×64, $\mu_p \simeq 4.4$. This shows that more terms of P_{S_r} are needed for short and wide fishnets than for the long and narrow ones. Due to the fact that the laws of stress redistribution around scattered failures are almost identical, the common terms of $P_{S_r}, r \leq r_0$, in P_f for both fishnets, are almost the same. The only difference is that the next few terms $P_{S_r}, r > r_0$ for the short and wide fishnets, are much larger than those for the long and narrow ones. The cause is the delay of damage localization.

4.5.5. Size effect on fishnet strength

Like all quasibrittle materials, fishnets exhibit a strong size effect, which is both statistical, due to random link strength, and deterministic, due to stress redistributions, the latter caused by the fact that the stress redistribution affects a relatively smaller zone in larger fishnet. To study it, we must change size D while keeping geometric similarity, i.e., keeping constant the aspect ratio k/n of the fishnet. Length n may serve as the size, D. Then we calculate the change of the mean (or median) strength $\bar{\sigma}_N$ as size D is varied, and plot $\log \bar{\sigma}_N$ (or $\log \sigma_{0.5}$) vs. $\log D$.

Consider now two square fishnets ($k = n$) with sizes D_0 and $2D_0$. The schematic illustrations of P_f in Weibull scale are, for both sizes, shown in Fig. 18a. Recall that the upper tail of the P_f curve is asymptotically identical to the finite weakest-link model with the same number of links, and so the increase of the number of links due to doubling of the size will shift the graph upward at the upper tail. On the other hand, more scattered failures of links take place before the peak load of a larger structure, which makes the lower tail of the P_f curve steeper and causes the size effect curves for different sizes to cross (as seen in Fig. 18). This is qualitatively different from the evolution of cdf curves with increasing structure size in Type 1 failures of quasibrittle particulate or composite materials (Bažant and Le, 2017, Hoover and Bažant, 2014), for which such crossing cannot occur.

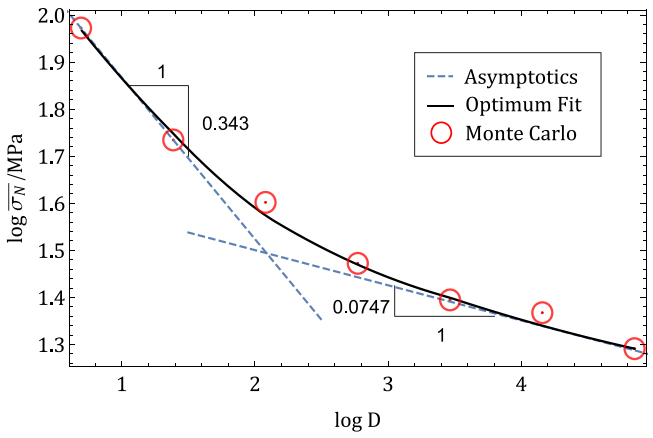

Fig. 19. Statistical size effect of square fishnet on the mean strength computed for sizes $D = 2, 4, 8, \ldots, 128$. Each $\bar{\sigma}_N$ gives the mean strength of random 10 samples of the same size.

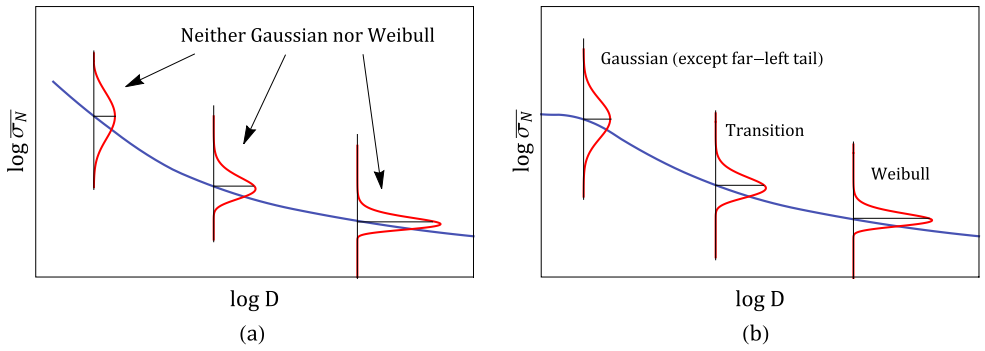

Fig. 20. a) Statistical size effect on mean strength of fishnet; b) Type I statistical size effect on mean strength.

Since the median is close to the mean and needs less computations, we further use the median and find it simply as the ordinate at which the coordinate is 0.5. Then the portion of cdf curve near the mean can be approximated by the tangent (Weibull line) through the point $x = \ln \bar{\sigma}_N$. The approximation by Weibull distribution is, of course, far from accurate at both cdf tails of P_f, but since the contribution of tails to the mean are negligible, this approximation is still very accurate for the mean as well as median. We know that the size effect curve of Weibull distribution (Bažant and Le, 2017) is a straight line with slope $-2/m$ for 2D structures.

Using this Weibull approximation for the cdf of fishnet P_f, the slope of the size effect curve at a fixed size D equals $-2/m$, where m is the slope of the tangent in the Weibull plot of the cdf of P_f (see Fig. 18a and b). As D increases from D_0 to $2D_0$, the Weibull modulus m of the linear approximation near the mean (or median) will increase from m_1 to m_2. Therefore, the slope of mean strength in Fig. 18b will increase from $-2/m_1$ to $-2/m_2$ and, correspondingly, the curve becomes flatter as size D increases.

To verify the foregoing qualitative behavior of the size effect curve, we run Monte Carlo simulations for square fishnets of different sizes ($D = 2, 4, 8, \cdots, 128$). For each size, the sample mean $\bar{\sigma}_N$ is calculated from 10 results of simulation. The resulting size effect curve is shown in Fig. 19. It verifies the aforementioned qualitative conclusion. The slope decreases from 0.343 to 0.0747 as the fishnet size D increases from $k = 2$ to 128.

Note that the statistical size effect of fishnet is quite similar to the type I size effect of quasi-brittle materials (Bažant and Le, 2017; Grassl and Bažant, 2009), whose deviation from Weibull type size effect is mainly due to the finite size of the RVE, which must fail before the structure fails. In both cases, the CoV of fishnet strength decreases with increasing size, and the cdf skewness varies from negligible at small sizes and to high (and of the same sign) at large sizes (Fig. 20b).

There is, however, an important difference from non-lamellar quasibrittle materials: The fishnets do not possess a fixed-size RVE, whose failure would cause the whole structure to fail. For a nearly deterministic fishnet (or a very small CoV of link strength), the fishnet failure is decided by the rupture of a single link (like in Type 1 quasibrittle failures), while for an increasing randomness (or an increasing CoV of the link strength), more and more scattered link failures will occur before the damage localizes and causes overall failure.

Another difference (Fig. 20) is that the distribution of P_f for rectangular fishnets of a fixed shape (except $k/n \to 0$ or ∞) can be neither Weibull nor Gaussian for any size. By contrast, for type I size effect, the cdf of P_f is Gaussian for small sizes (except the far-out left tail), and Weibullian for very large sizes.

4.6. Comparison with the chain of bundles

Attempts have previously been made (e.g. Harlow and Phoenix, 1978a; 1978b; Wei et al., 2015) to use a chain of fiber bundles to model the failure probability of unidirectional fiber composites under uniaxial tension. A long specimen under uniaxial tension is subdivided, by imagined cross sections of some assumed spacing, into fictitious segments, each of which is modeled as a fiber bundle. This is an approach that has an approximate physical justification in the microstructure of unidirectional fiber composites but not of nacreous materials.

If a fiber bundle with equal load sharing is represented mechanically by loading through rigid platelets, each parallel coupling reduces the reach of a power law tail by about one order of magnitude (Bažant and Le, 2017; Bažant and Pang, 2006). For 10 parallel fibers, the distribution becomes Gaussian except for a power law (or Weibull) tail reaching to the probability of only about 10^{-20}. The parallel coupling of fibers extends the reach of the Weibull tail (Bažant and Le, 2017; Bažant and Pang, 2006), but about 10^{22} bundles in the chain would be needed to approach the Weibull distribution expected for a very long structure. Obviously, such mechanics based equal load-sharing hypothesis gives clearly unreasonable predictions.

The problem with power law (or Weibull) tail shortening is avoided by some convenient but purely intuitive load-sharing rules for the transfer of load from a failed fiber to its neighbors. A convenient load-sharing rule can give a very different probability distribution G_n for each bundle, with a realistic reach of power law tail even though the load-sharing rule is not realistic. Like the fishnet, a chain of bundles, each with a suitable G_n, can then predict, for low probabilities, a reasonable slope increase in the low-probability range of Weibull plot, as shown by Harlow and Phoenix (1978a, 1978b).

In the fishnet model, by contrast, this slope decrease is engendered by the addition of non-zero probabilities P_{S_r} of structure survival, corresponding to maximum loads reached after the failure of r links. The slope of P_f will increase, at least by a factor of 2, due to adding the first term, P_{S_1}. As mentioned before, adding more terms P_{S_r} increases the slope further.

Importantly, the fishnet model needs no separate hypothesis about transverse load sharing or redistribution, to reproduce the aforementioned behavior.

5. Conclusions

1. The failure statistics of nacre-like material with imbricated (or staggered) lamellar microstructure under longitudinal tension can be approximately modeled by square fishnets pulled diagonally.
2. The probability distribution of fishnet strength, including the far-out left tail, can be calculated as a series of failure probabilities for maximum load occurring after the failure of one, two, three, etc., links. The series converges rapidly—the faster the greater the coefficient of variation (CoV) of scatter of each link.
3. The terms of this series represent various combinations of joint probabilities of survival and additive probabilities of failure for disjoint events. Near the zone of failed links, the link survival probabilities must be modified according to the mechanical stress redistribution due to previously failed links. The autocorrelation length of the link strength field is assumed to be equal to the link size and, therefore, is not considered.
4. In contrast to the weakest-link model for Type 1 quasibrittle failures of particulate materials, there is no fixed-size representative volume element of material (RVE). The size of the zone of failed links at maximum load increases with the CoV of link strength.
5. Compared to probability distribution for the finite weakest-link model developed for particulate materials and fiber composites, the strength at the failure probability level $P_f = 10^{-6}$ is about 11% higher, whereas at fixed load the failure probability is about 25-times lower, in terms of the ratio of strength to the mean strength. This ratio increases with increasing CoV of strength scatter of each link, but at the same time the mean strength decreases. Thus the combined effect at the level of $P_f = 10^{-6}$ is not necessarily strength decrease. It could be strength increase.
6. In contrast to finite weakest-link model for Type 1 failures, the fishnet shape, i.e., the width-to-length aspect ratio, has a major effect on the probability distribution of strength. The greater this ratio, the higher is the safety margin, i.e., the greater is the strength at the failure probability level $P_f = 10^{-6}$.
7. The nominal strength of fishnet at the same width-to-length ratio decreases significantly with the fishnet size. The size effect law is similar, though not the same, as in quasibrittle Type 1 finite weakest-link model.
8. There is a strong size effect, similar to, though different from, the finite weakest-link model for Type 1 quasibrittle size effect characterizing particulate or granular materials and fiber composites. The evolution of cdf curves shows that, with increasing structure size, the cdf curves in Weibull scale get progressively steeper and cross each other, which is a qualitative difference from quasibrittle particulate or composite materials.
9. Increasing the aspect ratio from 0 to ∞, the fishnet gradually transits for the weakest-link chain to the fiber bundle as the limit cases.
10. The model is verified by about a million Monte Carlo simulations of fishnet failure, for each of many different aspect ratios, link strength CoVs and fishnet sizes.
11. A similar steepening of the distribution slope at the lower end of Weibull scale plot can also be achieved by the chain-of-bundles model, but only if a convenient intuitive non-mechanical load-sharing rule is empirically postulated for each bundle, and if the specimen length is subdivided by chosen cross sections into statistically independent segments of suitable length, corresponding to each bundle. The imbricated (staggered) lamellar connectivity cannot be captured.
12. There are now three basic, analytically tractable, statistical models for the strength of materials and structures:

- the weakest-link chain model (series coupling),
- the fiber bundle model (parallel coupling), and
- the fishnet model (imbricated, or mixed, coupling)

The third includes the first two as the limit cases.

Acknowledgments

Partial support from the Army Research Office Grant W911NF-15-1-0240 is gratefully acknowledged. Some preliminary studies also drew support from NSF Grant CMS-0556323.

References

Alava, M.J., Nukala, P.K., Zapperi, S., 2006. Statistical models of fracture. Adv. Phys. 55 (3–4), 349–476.
Askarinejad, S., Rahbar, N., 2015. Toughening mechanisms in bioinspired multilayered materials. J. R. Soc. Interface 12 (102), 20140855.
Bažant, Z.P., 2005. Scaling of Structural Strength, second ed. Elsevier, London.
Bažant, Z.P., Le, J.-L., 2009. Nano-mechanics based modeling of lifetime distribution of quasibrittle structures. Eng. Failure Anal. 16 (8), 2521–2529.
Bažant, Z.P., Le, J.-L., 2017. Probabilistic Mechanics of Quasibrittle Structures: Strength, Lifetime, and Size Effect. Cambridge University Press, Cambridge, U.K.. (ISBN 978-1-107-15170-3)
Bažant, Z.P., Le, J.-L., Bazant, M.Z., 2009. Scaling of strength and lifetime probability distributions of quasibrittle structures based on atomistic fracture mechanics. Proc. Nat. Acad. Sci. 106 (28), 11484–11489.
Bažant, Z.P., Pang, S.-D., 2006. Mechanics-based statistics of failure risk of quasibrittle structures and size effect on safety factors. Proc. Nat. Acad. Sci. 103 (25), 9434–9439.
Bažant, Z.P., Pang, S.-D., 2007. Activation energy based extreme value statistics and size effect in brittle and quasibrittle fracture. J. Mech. Phys. Solids 55 (1), 91–131.
Bažant, Z.P., Planas, J., 1998. Fracture and Size Effect in Concrete and Other Quasibrittle materials. CRC Press, Boca Raton, FL.
Bažant, Z.P., Xi, Y., 1991. Statistical size effect in quasi-brittle structures: II. Nonlocal theory. J. Eng. Mech. 117 (11), 2623–2640.
Bertalan, Z., Shekhawat, A., Sethna, J.P., Zapperi, S., 2014. Fracture strength: stress concentration, extreme value statistics, and the fate of the weibull distribution. Phys. Rev. Appl. 2 (3), 034008.
Daniels, H.E., 1945. The statistical theory of the strength of bundles of threads. I. Proc. R. Soc. London A 183 (995), 405–435.
Dutta, A., Tekalur, S.A., Miklavcic, M., 2013. Optimal overlap length in staggered architecture composites under dynamic loading conditions. Journal of the Mechanics and Physics of Solids 61 (1), 145–160.
Dutta, A., Tekalur, S.A., 2014. Crack tortuousity in the nacreous layer–Topological dependence and biomimetic design guideline. International Journal of Solids and Structures 51 (2), 325–335.
Fisher, R.A., Tippett, L.H.C., 1928. Limiting forms of the frequency distribution of the largest or smallest member of a sample. Math. Proc. Cambridge Philos. Soc. 24 (02), 180–190. Cambridge University Press.
Gao, H., Ji, B., Jäger, I.L., Arzt, E., Fratzl, P., 2003. Materials become insensitive to flaws at nanoscale: lessons from nature. Proc. Nat. Acad. Sci. 100 (10), 5597–5600.
Grassl, P., Bažant, Z.P., 2009. Random lattice-particle simulation of statistical size effect in quasi-brittle structures failing at crack initiation. J. Eng. Mech. 135 (2), 85–92.
Harlow, D.G., Phoenix, S.L., 1978. The chain-of-bundles probability model for the strength of fibrous materials I: analysis and conjectures. J. Compos. Mater. 12 (2), 195–214.
Harlow, D.G., Phoenix, S.L., 1978. The chain-of-bundles probability model for the strength of fibrous materials II: a numerical study of convergence. J. Compos. Mater. 12 (3), 314–334.
Hoover, C.G., Bažant, Z.P., 2014. Cohesive crack, size effect, crack band and work-of-fracture models compared to comprehensive concrete fracture tests. Int. J. Fract. 187 (1), 133–143.
Le, J.-L., Bažant, Z.P., 2010. Scaling of strength of metal-composite joints: II. Interface fracture analysis. ASME J. of Applied Mechanics 77, 011012-1–011012-7.
Le, J.-L., Bažant, Z.P., 2009. Finite weakest-link model with zero threshold for strength distribution of dental restorative ceramics. Dental Mater. 25 (5), 641–648.
Le, J.-L., Bažant, Z.P., 2011. Unified nano-mechanics based probabilistic theory of quasibrittle and brittle structures: II. Fatigue crack growth, lifetime and scaling. J. Mech. Phys. Solids 59, 1322–1337.
Le, J.-L., Bažant, Z.P., 2012. Scaling of static fracture of quasi-brittle structures: strength, lifetime, and fracture kinetics. J. Appl. Mech. 79 (3), 031006.
Le, J.-L., Bažant, Z.P., Bazant, M.Z., 2009. Subcritical crack growth law and its consequences for lifetime statistics and size effect of quasibrittle structures. J. Phys. D 42 (21), 214008.
Le, J.-L., Bažant, Z.P., Bazant, M.Z., 2011. Unified nano-mechanics based probabilistic theory of quasibrittle and brittle structures: I. Strength, static crack growth, lifetime and scaling. J. Mech. Phys. Solids 59 (7), 1291–1321.
Luo, W., Bažant, Z. P., 2017. Fishnet statistics for strength scaling of nacreous imbricated lamellar materials. ArXiv preprint arXiv:1706.01591(June 4).
Pang, S.-D., Bažant, Z.P., Le, J.-L., 2008. Statistics of strength of ceramics: finite weakest-link model and necessity of zero threshold. Int. J. Fract. 154 (1), 131–145.
Salviato, M., Bažant, Z.P., 2014. The asymptotic stochastic strength of bundles of elements exhibiting general stress? Strain laws. Probab. Eng. Mech. 36, 1–7.
Salviato, M., Kirane, K., Bažant, Z.P., 2014. Statistical distribution and size effect of residual strength of quasibrittle materials after a period of constant load. J. Mech. Phys. Solids 64, 440–454.
Shao, Y., Zhao, H.P., Feng, X.Q., Gao, H., 2012. Discontinuous crack-bridging model for fracture toughness analysis of nacre. J. Mech. Phys. Solids 60 (8), 1400–1419.
Wang, R.Z., Suo, Z., Evans, A.G., Yao, N., Aksay, I.A., 2001. Deformation mechanisms in nacre. J. Mater. Res. 16 (09), 2485–2493.
Wei, X., Filleter, T., Espinosa, H.D., 2015. Statistical shear lag model: unraveling the size effect in hierarchical composites. Acta Biomater. 18, 206–212.